DEVELOPMENT, TESTING AND CHARACTERIZATION OF ELECTRONIC SKINS FOR ROBOTS

by

RITVIJ SAHASRABUDDHE

Presented to the Faculty of the Graduate School of

The University of Texas at Arlington in Partial Fulfillment

of the Requirements

for the Degree of

MASTER OF SCIENCE IN ELECTRICAL ENGINEERING

THE UNIVERSITY OF TEXAS AT ARLINGTON

December 2015

Copyright © by Ritvij Sahasrabuddhe 2015

All Rights Reserved

Acknowledgements

First, I would like to thank Dr. Popa for giving me an opportunity to work with him. I am grateful to him for his endless support, for believing in me and constantly motivating me to achieve my project goals. It was a pleasure to work with him and the Next Generation Systems Group. I would like to thank my defense committee members Dr. Lewis and Dr. Magnusson for their valuable time to attend my thesis defense without giving a second thought. Thanks to Dr. Lee for his guidance and support. I am thankful to The University of Texas at Arlington and UT Arlington Research Institute (UTARI) for providing me with the best facilities and infrastructure to carry out my thesis work.

My sincere thanks to my parents: Ravindra Sahasrabuddhe and Rijuta Sahasrabuddhe for their never ending support, love and sacrifices. I wish to thank my brother Hrishikesh and sister-in-law Reema for guiding, inspiring and encouraging me to successfully pursue my master's degree.

My special thanks to Fahad Mirza, Joshua Baptist and Sumit Das for guiding and helping me throughout my research work. I would also like to thank my all NGS Lab colleagues especially, Abhishek Thakurdesai, Isura Ranatunga, Sandesh Gowda, Sven Cremer, Dr. Indika Wijayasinghe and Namrata Balakrishnan for their strong support.

This work was supported in part by National Science Foundation NRI Grant #IIS-1208623.

November 19, 2015

Abstract

DEVELOPMENT, TESTING AND CHARACTERIZATION OF ELECTRONIC SKINS FOR ROBOTS

Ritvij Sahasrabuddhe, MS

The University of Texas at Arlington, 2015

Supervising Professor: Dan O. Popa

The main purpose of this thesis is to test and characterize newly developed pressure sensors integrated into robot skin and understand their behavior for different testing parameters such as sensor and skin materials and geometry. Flexible electronic skin is meant to behave similar to human skin acting as a tactile interface with the robot environment. Before placing electronic skin onto robots, it is important to test and characterize such structures. Since the behavior of our pressure sensors embedded in robot skin was still unknown, an experimental setup has been developed in order to test and characterize the sensors and collect the real time data.

The experimental setup described in this thesis includes various hardware systems such as a National Instrument's cRIO real time controller, a load cell and a plunger attached to a linear actuator to gathers the real time pressure measurements. The test process was automated using custom software written in LabVIEW which not only gathers the data in real time but also increases the speed of operation. Different force control algorithms were implemented, which safely achieve the robot-environment interaction.

Along with the sensors, different skin types were tested and characterized based on the experimental data gathered from the system. After data analysis, a particular combination of skins and sensors was chosen as most promising for further studies.

Table of Contents

List of Illustrations

Chapter 1

Introduction

1.1 Motivation for Characterization of Electronic skins

To perform the specific and dedicated industrial tasks, robots have been widely used for the last 50 years. They are capable of performing numerous dedicated tasks with high precision repeatability and accuracy. The contact interaction between the robot and human or any other object is an important safety factor to consider when deploying robots in industry. Until a few years ago, robots were considered to be useful only in few manufacturing industries such as automobile welding or electronic chip packaging [1]. But in recent years, there is a growing need for robots that mimic and perceive the environmental or surrounding effects just like human. To achieve this, researchers have proposed developing human-like sensor skins for robots, which are expected to perform similar role as human skin, and thereby increase the tactile awareness of the robot to external pressure stimuli [2]. Future human-like robots are expected to be more complex than the other robots as they are likely to resemble human skin properties, or the intelligence to adapt to the environmental and other surrounding situations [1].

Scientists have been researching on making multimodal skins consisting of sensors such as pressure, temperature and touch. These sensors are broadly called tactile sensors. Due to addition of these multimodal functionalities, the robot skin acts just like a human skin by acting as an interface to the environment [3] [4]. To gather the information from an environment or to interact with it, the electronic skin, more importantly the sensors integrated on it, play a major role.

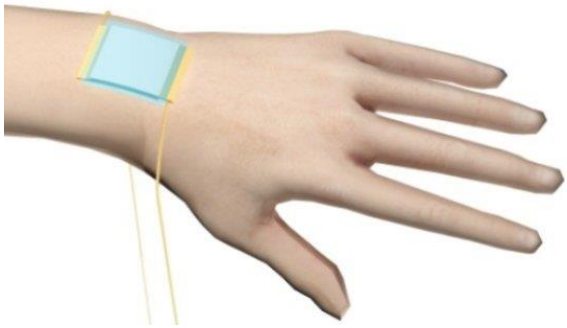

Figure 1 – Flexible Electronic skin with multidimensional capabilities [5]

Electronic skins have to be designed carefully by considering various factors, such as efficient sensor placement, bandwidth, resolution and density. These parameters need to be inspected even before they are integrated on the robot body. To make this process easier and better, robot skin models should be developed for better understanding of electronic skin structure. It also helps curtail the time taken for running the iterations to design them. For this purpose, the Next Generation Systems Group (NGS) at the University of Texas at Arlington is currently developing the skin simulation environment known as SkinSim, and has prototyped pressure sensitive skins embedded in silicone and Frubber® elastomers as described in this project.

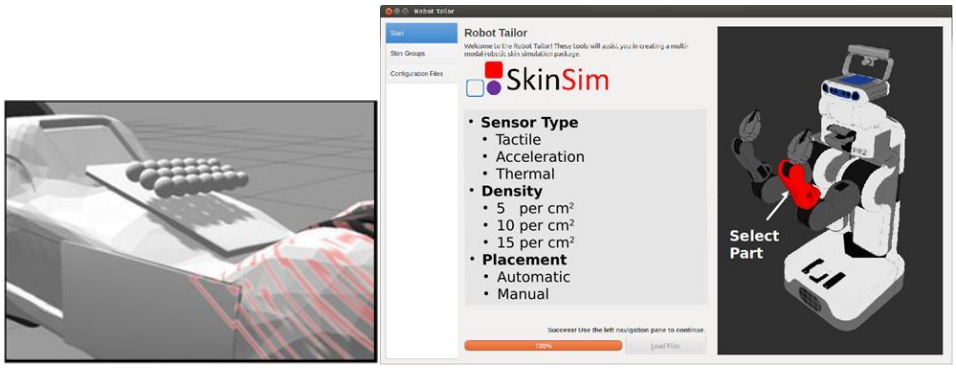

Figure 2 – SkinSim simulation environment [6]

SkinSim is a simulation environment developed for the better understanding of design optimization of robot skin parameters [6]. In this simulated environment, the realistic reduced-order module of robot skin is being implemented. This model will help to relate the force data collected from embedded taxels to the force applied to the robot skin [7]. Using SkinSim, models can be created for different samples such as single sensor modules, arrays of sensors, robot skin type and the sensors integrated in skin samples.

1.2 Challenges

Tactile sensors are needed in current robot skin technology and are very important for the robot - environment interaction. The main transduction mechanisms for these sensors are: piezoresistive and capacitive. However, there are drawbacks to use both types of sensor. For piezoresistive pressure sensors, challenges include rigidity, temperature sensitivity and fragility [8] [9]. Due to the temperature sensitive nature of the sensors, the resistance output of the sensor changes if it is not kept under constant ambient temperature conditions which makes it difficult to identify the intrinsic behavior of the newly developed sensors.

Both piezoresistive and capacitive sensors experience drift in their response. All these sensors experience low or high amount of drifts – irrespective of how accurate they are, what type of material used to fabricate them or how expensive they are. The drift in sensors is nothing but the gradual degradation in their output response observed over the time with respect to their pre-calibrated response readings. Another important factor to be considered is hysteresis. The hysteresis phenomenon refers to the unfaithful repeatability of the sensor’s response which is observed and compared when the sensors are experiencing loading and unloading [10]. It basically shows a different relationship between system’s input and output during loading and unloading.

Depending upon the material used, the physical properties of pressure sensors change, which might result in different sensor responses when exposed to similar conditions [10]. The change in environmental conditions, material responses and changes in loading profiles result in drift in the output response of the sensor. The amount of drift varies from sensor to sensor.

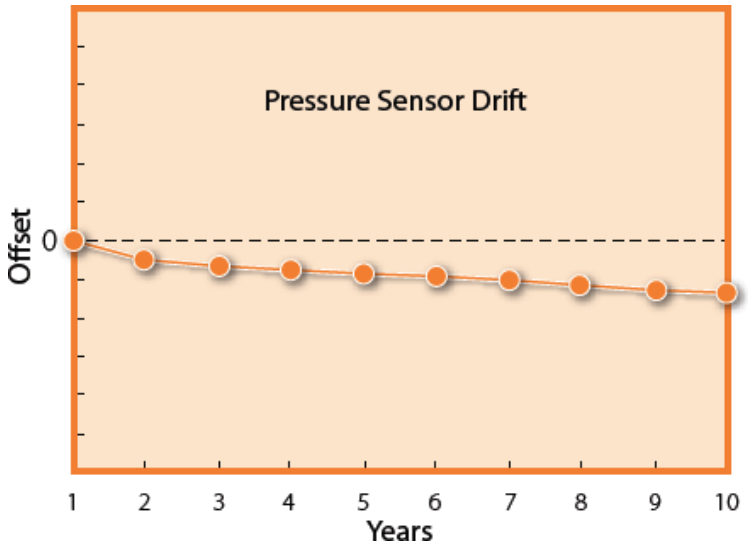

Figure 3 – Example of Sensor drift over the time [10].

The tactile sensor-to-sensor variation could be observed not only for the sensors of the different types but also for the different sensors of the same type. For this reason each and every sensor has to undergo calibration tests. The calibration tests give the desired zero set point and also the desired specifications. These calibration tests must be performed under carefully controlled surrounding and experimental conditions for each sensor unit.

Considering the different types of tactile sensors modules, an experimental setup has been developed in this work to be suitable for all such modules. It is important that the experimental setup must include the appropriate fixtures to perform the experiments.

The model fitting for tactile modules has to be done based on an appropriate method that takes into account their nonlinear behavior. Since there could be different materials or physical properties used for making the tactile skin, different methods of parameter identification and model fitting should be investigated. To check if the model identification is done properly or consistent for a particular tactile module, it is best to apply different model identification methods and compare them to ensure the repeatability.

1.3 Details of work conducted

The main goal of this thesis is to test and characterize newly developed piezoresistive pressure sensors. Piezoresistive pressure sensors were manufactured at the University of Texas at Arlington using microstructuring technology. This thesis work is focused on a part of manufacturing process for sensors (EHD Printing) and the characterization tasks after sensor packaging, in particular force indentation experiments.

After substrate fabrication in the clean room, the sensor substrate undergoes the printing process. In this project, the Electrohydrodynamic (EHD) inkjet printing process was used to print on the sensors. The main reasons for choosing the EHD printing are that it supports the wide range of materials as well as it can print the higher viscosity materials of up to 1000cP, much higher when compared to maximum 50cP using conventional printing process [11]. The first step in EHD printing was to prepare the inks. The sensors can be categorized based on the ink materials used to print on the sensors. Here, the Poly (3, 4-ethylenedioxythiophene): Polystyrene sulfonate (PEDOT: PSS) is used as piezoresistive element in the ink. By keeping PEDOT: PSS as a base element, two types of inks were prepared based on two different solvents viz. – NMP (1-Methyl-2-pyrrolidinone) and DMSO (Dimethyl Sulfoxide). Based on the two inks – PEDOT: NMP (1:2 ratio) and PEDOT: DMSO (1:3 ratio), the sensors can be categorized as NMP

sensor and DMSO sensor. Furthermore, the sensors were categorized based on the number of ink layers printed on it.

After printing, in order to test and characterize the sensors, an existing experimental testbed at UTARI labs was modified according to the need of newly developed sensors. The hardware includes National instrument's cRIO 9074 controller, and the x-y stage with linear actuator mounted with encoder feedback mounted vertically on top of x-y stage [7]. The TTI load cell is mounted on the actuator through which the applied force on the sensors can be measured. The NI servo drive module connected through Maxon servo amplifier was used to control the linear actuator. The linear actuator, with plunger attached to it, was used to perform experiments by indenting into the skin material and the pressure sensors. The additional circuitry used to process the signal obtained from the sensors. The Wheatstone bridge along with instrumentation amplifier was used to measure the unknown resistance output from sensors and amplify the voltage output before reading it to through the controller. To carry out the different tests on the sensors, the sensors were placed on the x-y stage. The plunger position was aligned to reach either on top of the sensors or to the desired position around the sensors depending upon the requirements of particular experiments. The skin samples of different types and thicknesses were used and fixed at the top and bottom of the sensors. Wide range of experiments were performed by taking into account the different combinations of placement of skin samples with different thicknesses. Skin samples were used along with sensors, with different combinations, such as skin at the bottom and at the top of the sensors, skin only at top and skin only at bottom of the sensors.

The important part of this thesis includes the automated testing and characterization of pressure sensors. To automate the process, different LabVIEW programs were created. Using LabVIEW, the motion of linear actuator is controlled and

the real time measurements were gathered from the Load cell and the pressure sensors. The automation programs were created to carry out various tests on the sensors such as Sinusoidal motion profile, square wave motion profile, application of different force with different frequency ranges, application of continuous force and different static tests which includes applied force increments in steps. All these tests were automated and combined in just one LabVIEW VI. So the user just needs to mention the required force, frequencies and motion profiles and the whole process would be completed without user intervention. The LabVIEW programs were also created to automate the file saving process. Previously, the data obtained from the sensors was stored in file which was saved in cRIO memory. As the cRIO has limited memory space, it was difficult to store all the files in cRIO. In addition to this, the file names had to be entered manually each time after creating the file. These problems are eliminated by automating the file saving process. Now the files are directly stored in Computer which eliminates the memory problem. Also, the program is written in such a way that it will automatically save the file name which includes the parameters used while performing the particular test. For example, if we use PEDOT: NMP sensor and apply 10N force with 5 Hz frequency with sinusoidal motion profile then it will automatically store the data in the file named as - "NMP_10N_5Hz_sinusoidal.csv".

The LabVIEW programs were also created for applying the force control algorithms on the sensors. Two main algorithms were developed, viz. – Explicit force control and Impedance control strategy. Explicit for control helped to apply to desired force on the sensors. Although this technique gives the better response, it results in chattering which could damage the micron sized pressure sensors. To overcome the problem of chattering, Impedance control scheme was studied and implemented using LabVIEW. Before that, the simulation results for Impedance control technique were

obtained using MATLAB. These results are illustrated further in chapter 4 of this document.

1.4 Research Contribution of Thesis

1.4.1 Automated Testing and Interface Hardware

After development of pressure sensors, the next part was to perform different tests on sensors and analyze their behavior. Different sensors, with combinations of skin materials at the top and bottom, require plenty of test cases to be developed for each pressure sensor module. Manual testing process is a time consuming process which also reduces effectiveness and efficiency of software testing. For this reason, an automated testing platform was developed which improves the software quality by increasing scope and depth of tests. Automation processes were developed using LabVIEW graphical programming language which can execute multiple test cases within single software run and can generate multiple data files. A unique name was assigned to each file, indicating the type of pressure sensor and testing parameters used for each particular test, as hundreds of files had to be generated for each sensor. To improve the efficiency of testing process, file saving part was also automated using LabVIEW, in order to get rid of time consuming file saving process.

Change in resistance output of pressure sensors, after an application of desired amount force, was very small of the order of few milliohms. To read and process small amount of change in resistance, a PCB was developed. This PCB mainly includes two important transducer circuits – a Wheatstone bridge and an instrumentation amplifier. Initially, the Wheatstone bridge was balanced by adjusting the value of variable potentiometer equal to the pressure sensor attached at an adjacent leg, which takes the voltage reading of Wheatstone bridge to reference zero value. The output signal is amplified using AD623 Instrumentation amplifier.

1.4.2 Test and Gather Data to Characterize Pressure Sensors

At the beginning of this work, behavior of newly developed pressure sensors was largely unknown. In order to identify how pressure sensors work, an extensive testing process had been carried out. Two types of tests were performed – Static tests and dynamic tests. In static tests an incrementally increasing force was applied with 2 Newton per step by keeping each step constant for certain duration in order to observe the steady state response from sensors. Dynamic tests involve an application of sinusoidal motion profile in which four sinusoidal motions were applied for each test with frequency of 1 Hz. Tests were performed by placing the skin material of different thicknesses above, and/or below pressure sensors. Data reported in Chapter 4 of this work suggests that a particular combination of sensor materials and geometries among those investigated has a better performance.

1.5 Thesis Organization

Chapter 2 starts the literature survey for the following areas – 1) Research related to electronic skin and sensing technology; 2) Research about different force control strategies including explicit force control, position control and impedance control; 3) Automation of x-y moving stage; 4) Research for Electrohydrodynamic (EHD) inkjet printing process which is advantageous over conventional printing processes.

Chapter 3 includes the information about the hardware and software used for this thesis. The experimental setup for testing and characterization of sensors is explained in detail and also, the hardware details are given for Electrohydrodynamic (EHD) inkjet printing process. The software part includes the programs written using both LabVIEW and MATLAB. LabVIEW programs to automate the process of testing and characterization of sensors are discussed in detail. In addition to this LabVIEW programs

for different force control strategies are also explained in detail. MATLAB program, used for simulation of impedance control scheme, is also discussed.

Chapter 4 gives the details about the experiments performed on the sensors in order to test and characterize them. Various factors were considered to perform the experiments on sensors such as – different skin types, application of range of forces, placement of skin material and sensor modules, size and shape of plunger used to apply the force on the sensors, different ink types classifying different sensor types and application of different loading profiles.

Chapter 5 draws conclusions based on the experiments performed to characterize the electronic skins and future research that could be done related to electronic skin characterization.

Chapter 2

Literature Survey

2.1 Research on Electronic Skin

The advancement in research related to the field of electronics and robotics has led to an innovative and impressive product called electronic skin. The electronic skin simply mimics the human skin with an addition of electronics embedded in it. Human skin, from an engineering point of view, acts as an interactive tool with the environment [3]. From the perspective of artificial intelligence, there is a direct contact with human and the biomedical applications in which prosthetic devices come in picture, the emergence of an electronic skin is a crucial outcome [12]. By taking this into consideration, researchers have developed an electronic skin which not only mimics some features of human skin but also empowers the idea of robot-environment interaction. These skins can be used to cover the whole part of the robots or machines.

Figure 4 – Flexible Electronic skin [13]

Touch is the most essential sense among the five senses of the body and also distributed throughout the body. It is possible to differentiate the spatial distances as low as about 40 micrometers using human's single fingertip [14]. The receptors in human's hand can sense as little pressure as 100 Pa and the pressures a lot more than 100 kPa.

This means human skin is very sensitive. For many years, researchers were trying to replicate these features of human skin in the artificial skin [3]. Some of them failed while some of them could make some progress replicating human skin features in electronic skin [15].

Along with replications of the sense features of human skin, the electronic skin should also be soft and flexible in order to be fitted on robots or machines of any shape. Flexible skin is easier to put on the outer surface of the body of the robots.

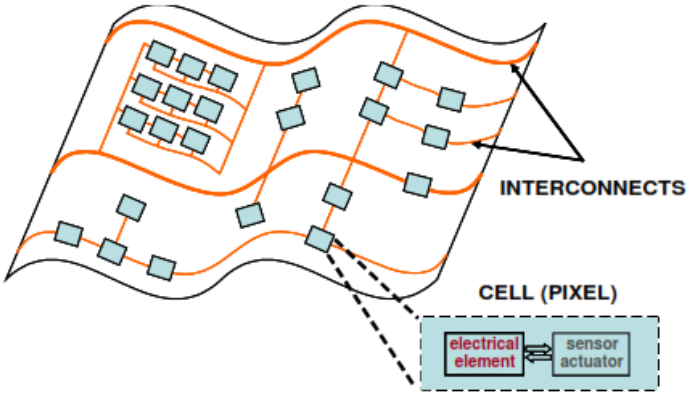

Figure 5– Concept of stretchable substrate carrying electronic circuits (figure adapted from [16])

The flexibility in electronic skin cannot be achieved with the semiconductor integrated circuits technology as it uses very stiff and rigid material for substrates [16]. For future benefits of robots and biomedical applications, the flexibility in electronic sensors or more specifically pressure sensors is very important as it helps to get better human-environment interaction [17]. The researchers at Princeton University have developed a flexible skin made up of transducers and other electronic circuits mounted on the flexible substrate that carries the maximum amount of strain which is illustrated in Figure 5 [16].

The next step in the development of the electronic skin will be the inclusion of multiple sensors having multiple features. The best example of active tactile modules is Hex-O- Skin. These sensors are designed and developed in such a way that they will sense not only the pressure but also temperature and acceleration. The future idea is all about developing the electronic skin with sensors of different types such as acceleration sensor, pressure sensor and temperature sensors. This will make the electronic skin smarter. HEX-O-SKIN has given a very redundant network structure of the sensor modules which adds robustness to its design.

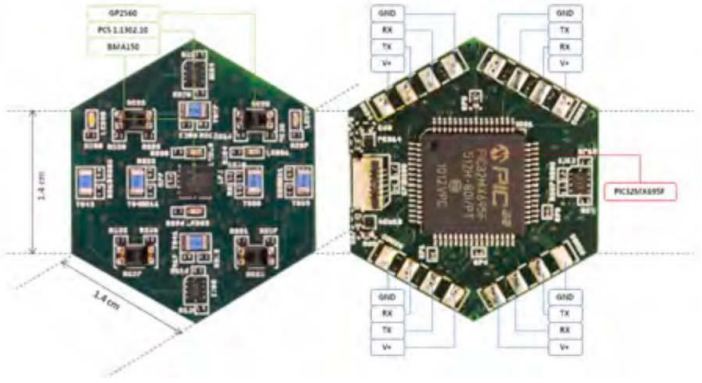

(a)

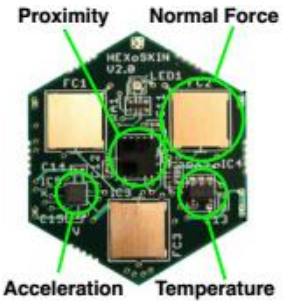

(b)

Figure 6 – a) HEX_O_SKIN with ports and size measures [18], b) HEXO_SKIN_O showing multiple sensors [19]

Mittendorfer et al. proposed the idea of developing the multimodal skin design in [18]. The HEX-O-SKIN is of hexagonal shape comprising multiple sensors as shown in Figure 6. All the sensors on this robot skin are connected to the local processor as can

be seen in Figure 6. The local controller is mounted on each HEX-O-SKIN module which preprocesses the sensor signals and directs those signals to the computer or host [18]. This module was developed along with the Field Programmable Gate Array. Mittendorfer presents three main features of the HEX-O-SKIN design in [18] – 1) A local ADC increases data integrity, 2) preprocessing decreases the necessary transfer and processing bandwidth and 3) active routing increases robustness.

Figure 7–Skin surface covered with HEX-O_SKIN modules [20]

Figure 7 shows how the HEX-O-SKIN modules are interconnected and placed on the robot's entire hand. Researchers have deployed these skins on KUKA and HRP2 robot. Although this technology looks attractive and advantageous, it yields many complexities in the design approach due to its topological skin nature and interconnection methods.

2.2 Research on Force Control methods

Nowadays, in most of the industrial applications, automation is becoming a notable trend. Automated manufacturing processes have become efficient after the emergence of force control technology. In many industrial applications, controlling the robots in contact with the environment is a critical problem and therefore, it is very

important to develop an appropriate force control scheme for different applications [21]. For the tasks which involves interaction with the environment, force control strategies give the strong and stable framework [22].

The basic structure of control system is represented in Figure 8. Any control system is a set of interconnections of various system components which gives the desired system response. The control system can be primarily categorized as open loop and closed loop control system. A closed-loop control system (Figure 8) uses the actual output response and compares it with the desired output response. The force control scheme uses the similar closed loop control strategy in order to maintain the desired contact force.

For many micro-scale applications, force control is a very important control strategy as it helps improve the efficiency of the response by giving an additional feedback output. The applications may include microassembly of medical and biological sensors. Force feedback response enables and ensures the safety of both assembly robot and the environment by controlling the interaction forces [23].

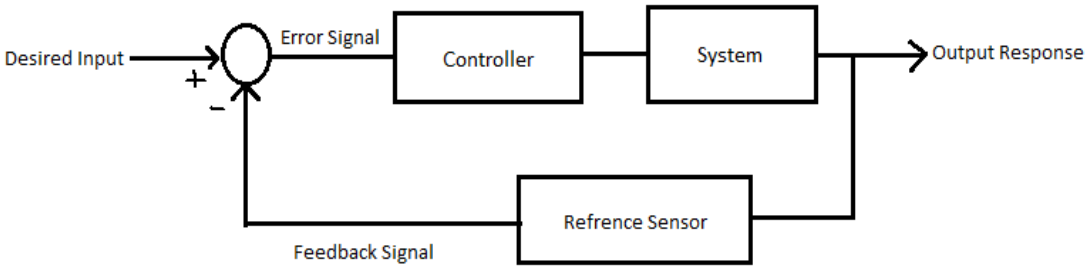

Figure 8 - Basic structure of a closed loop control system

Extensive past research has successfully proposed and validated force control strategies such as incremental force control and explicit force control [24]. In an incremental force controller, the desired force is compared with the measured force. The

comparison of desired and measured force gives an error force value. This value determines whether to increment or decrement the position. If the sign of the error is positive, the robot increments the position and applies the force in order to reach the desired force value and if the sign is negative, the robot decrements the position. This controller is easy to implement and robust. But, the response of this controller is very slow as the applied force takes time to reach the desired value. This is the main disadvantage of the Incremental force control.

Force control strategies can be divided into direct and indirect force control. Explicit force control is the most basic direct force control algorithm. This controller takes the direct commands measurements of the force values. In this the desired and measured force are compared with each other and the error signal is fed to the controller which processes it. After this, the processed signal is fed directly to the control system. This control scheme can be implemented with any one of the following controllers like P, PI, PD or PID. The explicit force control is the direct force control strategy.

Apart from these simple force control strategies, the work has been done for another control strategy known as position (stiffness) control. The tasks such as welding, spray painting which involves very less interaction between the robot and the environment, can be controlled using the position control strategies [25], [26], [27]. However, the applications such as assembly, grinding, polishing involves the considerable interaction between robots and environment. In this case, only controlling the position of manipulator is not desirable as it may result in damaging of robot or the object or both. Some researchers have considered variants of impedance control using recursive least squares [28]. This method estimates the mass, stiffness and damping of the unknown environment [28].

Raibert and Craig proposed the technique of hybrid force and position control [29]. This technique uses two separate loops to control the position and force. But, this technique is disadvantageous in case of unknown stiffness environment. Unexpected variations in stiffness of the environment are one the major factor being considered when there is a considerable interaction between a robot and the environment. To overcome the problem of unknown environment stiffness and to achieve a better stability with desired control behavior, the control technique called as an impedance control is suggested by many researchers [25]. This technique falls under indirect force control strategy.

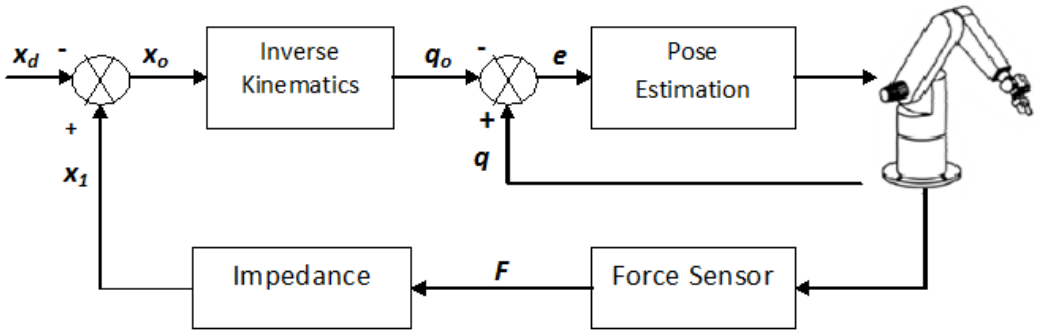

Figure 9– Impedance control scheme [30]

Impedance control technique provides the best force tracking control even when the environmental stiffness is unknown at the manipulator [31]. This strategy controls neither the force nor the position of the robot but their contact impedance along each direction. Researchers have developed the techniques by combining some or the other techniques mentioned above. Anderson and Spong used the hybrid Impedance control [28] which uses the switching control strategy. Villani, Chiaverini and Siciliano proposed the parallel control strategy with PI as inner force control loop in parallel with PD position control loop [29].

All these strategies mentioned above uses the switching of control between two or more control loops which causes the system to become unstable. So the new impedance control strategy is proposed which avoids the switching of control loops and still able to control both the inner position and outer force control loop.

2.3 Research in Electrohydrodynamic (EHD) printing

The manufacturing process of conductive patterning is of vital importance in current electronics industry [32]. There are various methods of fabrication techniques, one of them is lithography. But, lithography has its own disadvantages such as low throughput, time constraints etc. [32]. In case of flat surface structures, applying the lithography technique for more than two dimensional structures become very difficult and challenging [33]. Due to this some other technique needs to be taken into consideration. Non-lithographic methods such as roll-to-roll and inkjet can be used as fabrication methods which give better performance outcomes than that with lithography technique [32]. 3D printing was one of the suggested techniques by researchers. But there exists the problem of having low resolution in many of the new and current techniques which puts restrictions on developing complex 3D microstructures [33]. The modern fabrication method can be broadly divided into two different categories as Non-contact and Contact method. The EHD printing falls under Non-contact inkjet printing method which is capable of high speed processing. EHD printing offers the high printing resolution than other inkjet printing methods. It is an emerging printing technology having various advantages, such as maskless, high resolution and contactless, over conventional printing methods [34]. Also, the conventional printing methods are disadvantageous due to their limitations such as material deposition, viscosity of ink, flow rate, and the nozzle size [32]. These disadvantages of conventional printing strategies forced researchers to adapt Electrohydrodynamic printing which uses an electric energy to pull the ink out of the

nozzle [32]. Figure 10 shows the schematic of Electrohydrodynamic inkjet printing system. Further, the inkjet printers can be separated in two categories viz. Drop on demand, in which the drops are ejected from the nozzle at will, and the second is continuous, in which the droplets are ejected from the nozzle and break in stream of drops. The researchers claim that, this continuous method of printing sometime results in waste of an ink as it continuously injects the ink. So the EHD printing is enhanced with the advantages of manipulating the sizes of drops, frequency of ejection of ink.

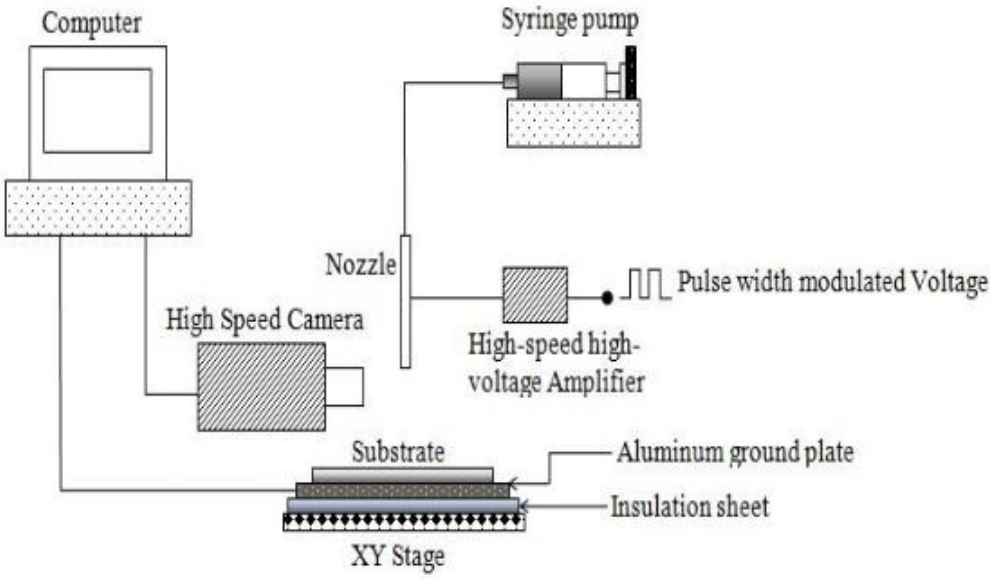

Figure 10– Setup of EHD Printing system [34]

In most of the traditional printing methods, the ink used to push out of the nozzle unlike the EHD printing, in which the liquid is pulled out from the nozzle [34].

2.4 Research in Automated Robotic Manipulation

As shown in Figure 10, EHD printing setup uses X-Y stage in order to align a sensor to perform EHD printing on it. Sensor alignment is very important as the error of even few microns may lead to the misprinting. Sensor alignment is done manually for each and every sensor to be printed. But, the process of the sensor alignment is very

tedious as the user has to move the x-y stage manually in order to minimize the error of the sensor orientation. Sensor alignment has to be done very precisely because even the smallest error or mistake could damage the sensor. The process suggested in [35] shows the advancement in sensor printing process. Figure 11 shows the representation of a Local co-ordinate frame with respect to Global co-ordinate frame. In this approach, the user does not need to align the sensor manually unlike the old method.

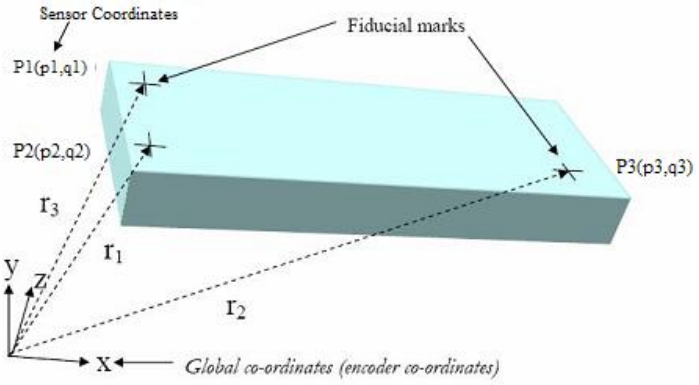

Figure 11– Frames representing Local and Global co-ordinates of XYZ stage [35]

The sensor can be placed in any orientation on the X-Y stage. The user acquires three fiducial points from the Local frame which simplify the mapping between two frames. This approach automates the process of sensor alignment for printing by mapping the co-ordinates of two frames [35]. This automation of EHD printing process is much faster than the manual process.

Chapter 3

Description of Hardware and Software

3.1 Hardware Setups

Two different experimental setups used for this thesis, one is for testing and characterization of pressure sensors and the other to print the pressure sensors using an Electrohydrodynamic (EHD) inkjet printing process. Various hardware components are involved in both the experimental setups. Apart from these two main setups, the PCB design and development has been done to build the sensor interfacing circuit. In this section, we will discuss each part of these setups

3.1.1 Experimental Setup for Sensor Testing

A Cartesian robot having the movable Z-axis is used to perform the experiments on the sensors. The linear actuator is mounted on the Cartesian robot for the movement in the direction of Z-axis. It is based on the Newport Stage system UTMCC1HL. In this project, two different sensors are used: the TTI-TMO1 load cell and the piezoresistive pressure sensor integrated on robot skin. The piezoresistive property states that the resistance changes with respect to the applied strain on the material. One can easily measure the change in applied and sensed voltage as the resistance changes. The main purpose of load cell is to give the measurements of applied force on the tactile sensors whereas the pressure sensor gives the sensed load as output. The actuator controls the movement of plunger which is used to apply the pressure on the sensors. It has a micrometer resolution which determines the linear actuator position down to the thousands of a micrometer The Newport stage system consists of motor and encoder. The system architecture of experimental setup is illustrated in Figure 13.

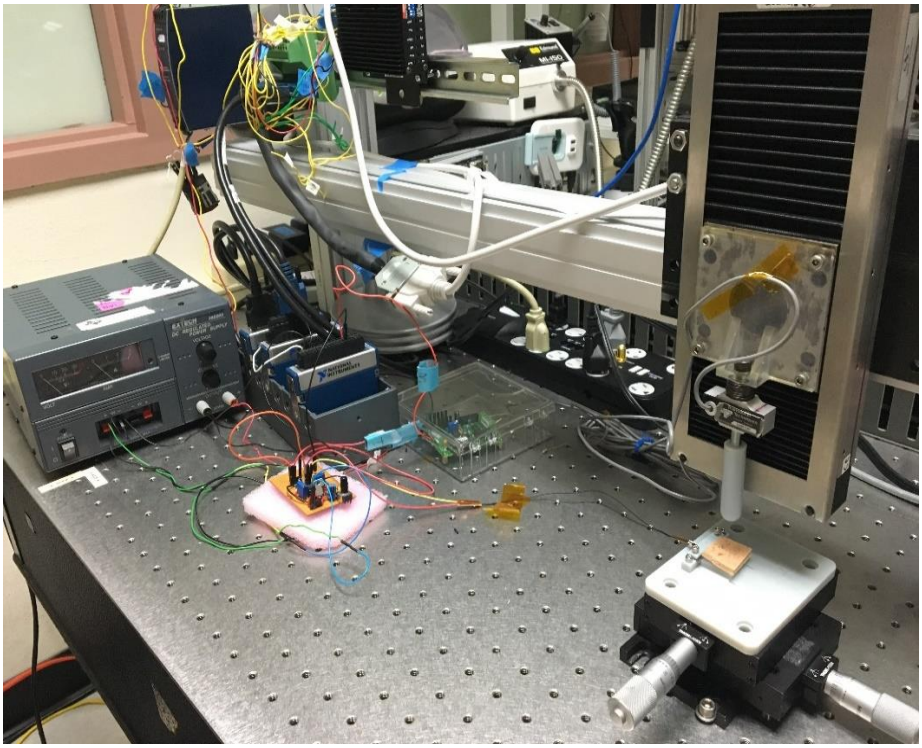

Figure 12– Experimental Setup for sensor testing

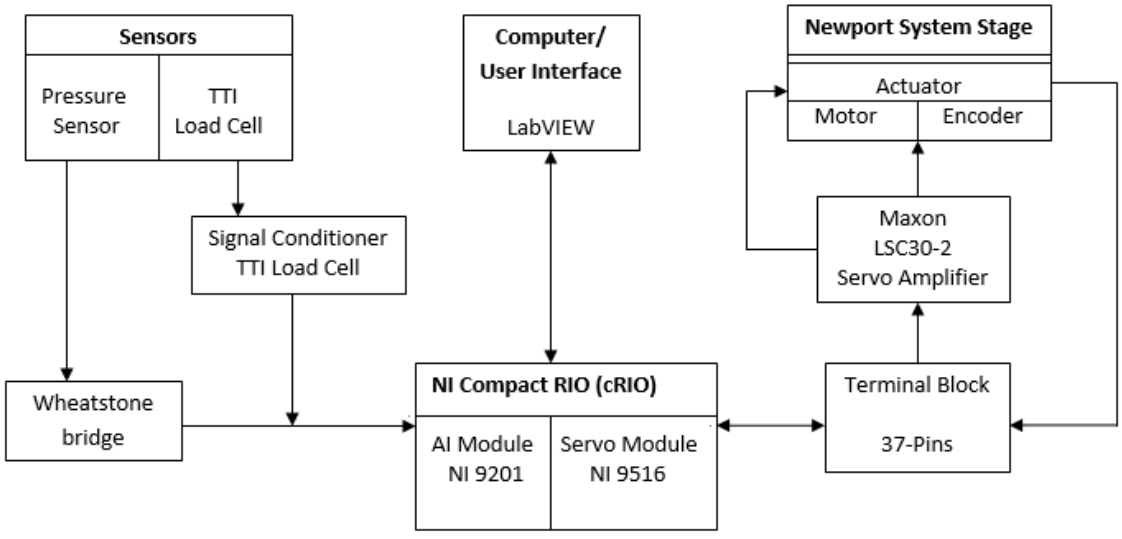

Figure 13– System architecture

The motor used to control the actuator is servo motor. Servo motor is a linear actuator that uses position feedback in order to precisely control the linear position, acceleration and velocity.

3.1.1.1 Real time controller and modules

In order to drive the Newport stage, some control mechanism is required. National Instrument's (NI) Compact RIO (cRIO) real time controller was used to control the actuator stage and also to collect the multiple data from the sensors in real time. Different models of cRIO are made available by National instruments. For this project cRIO 9074 model (shown in Figure 14 (a)) is used because of its simplicity and easy compatibility with most of the devices.

(a)

(b)

(c)

Figure 14– a) NI cRIO model No. 9074 [36], b) NI 9516 Servo Drive Interface [37], c) NI 9205 AI module [38]

The NI cRIO-9074 has a 400 MHz real-time processor along with a reconfigurable field-programmable gate array (FPGA) .It's FPGA chassis can accommodate 8for NI C Series hot swappable I/O modules. This controller has the ability to gather synchronous time-sensitive measurements from multiple sensors. The cRIO are controlled using the LabVIEW graphical programming language [39] [40]. LabVIEW is used not only to take the measurements but also to observe the corresponding real time waveforms. The operating range of cRIO is from -20 to 55 °C due to which it can be used for rugged applications. The cRIO 9074 gives an access to 512 MB of memory for data storage with 10/100Mb/s Ethernet port in order to achieve the programmable communication with PC [36].

In this setup, two NI C series I/O modules are used, first is NI 9516 servo drive interface(shown in Figure 14 (b)) and second is NI 9205 Analog input module (shown in Figure 14 (c)). The NI 9205 offers 16 differential and 32 single-ended analog inputs. Also, it has a sampling rate of 250kS/s with 16-bit resolution. Each channel has programmable input ranges of ±200 mV, ±1, ±5, and ±10 V. The NI 9205 has up to 60 V of overvoltage protection between input channels and common (COM) which gives protection against signal transients [38]. The analog module is used to get measurements from two sensors whereas NI 9516 has dual incremental encoder feedback setting which we can send the signals to and receive the signals from servo amplifier [37]. The signals coming out of NI 9516 are fed to Maxon servo amplifier [41] which sends the current signals to the actuator. After receiving the commands from actuator's encoder, the Maxon servo amplifier adjusts the current signal to reduce the position error.

3.1.1.2 Loading profile on sensors

The pressure sensor can be characterized using different methodologies. To perform testing operations, the specific setup had been created (shown in Figure 15).

The setup consists of Pressure sensors, Load cell to apply the force on the sensors, P10 silicon polymer skins to place at the bottom and top of the pressure sensor and controller and driver hardware to collect the experimental data in real time.

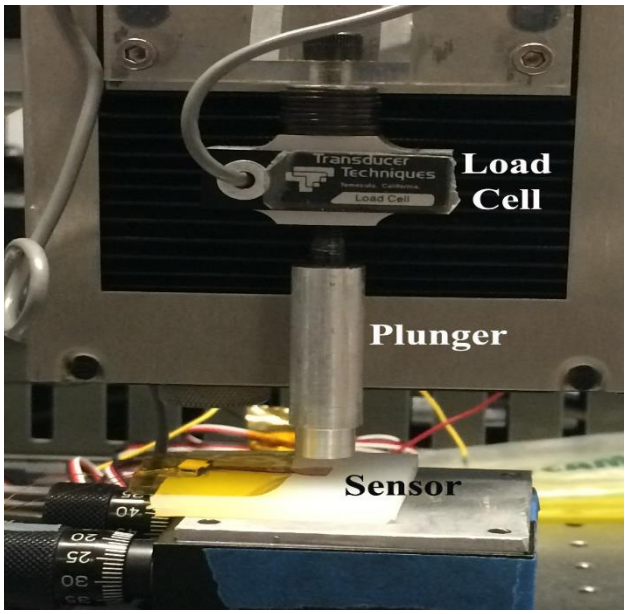

Figure 15– Test setup

To understand the behavior of the newly developed sensors, experiments were carried out in various fashions. Figure 16 a) and Figure 16 b) shows the difference between two methods of force application or loading profile. The Load cell along with plunger is used to apply the desired force on the sensors. The pressure sensor is placed on the 4mm P10 silicon polymer skin material.

Figure 16 a) shows how the force is applied exactly on top of the sensor. Due to this loading profile, the interdigitated structure of the sensor compresses. As per the property of strain gauge, the compression results in a decrease in resistance of the sensor and hence an increase in the corresponding voltage. Thus, the sensor output tries to follow the applied force trajectory. This helps to achieve the linearity in the sensor response as it varies approximately linearly with applied force.

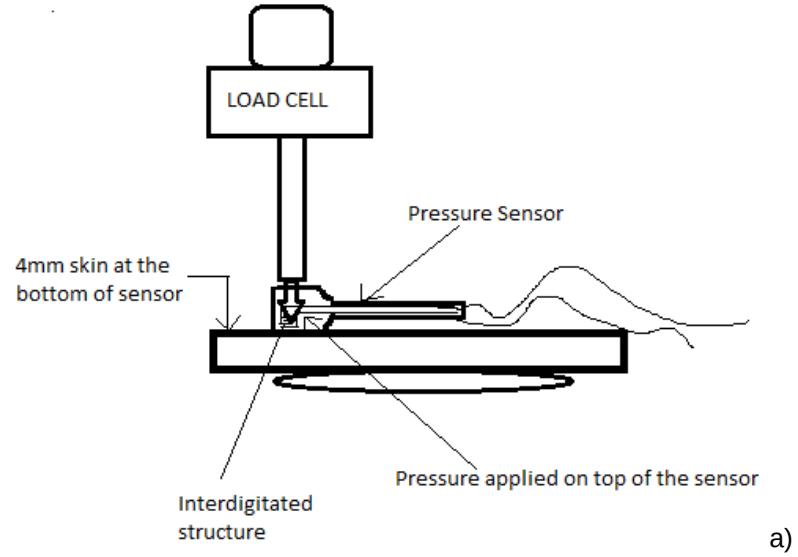

a)

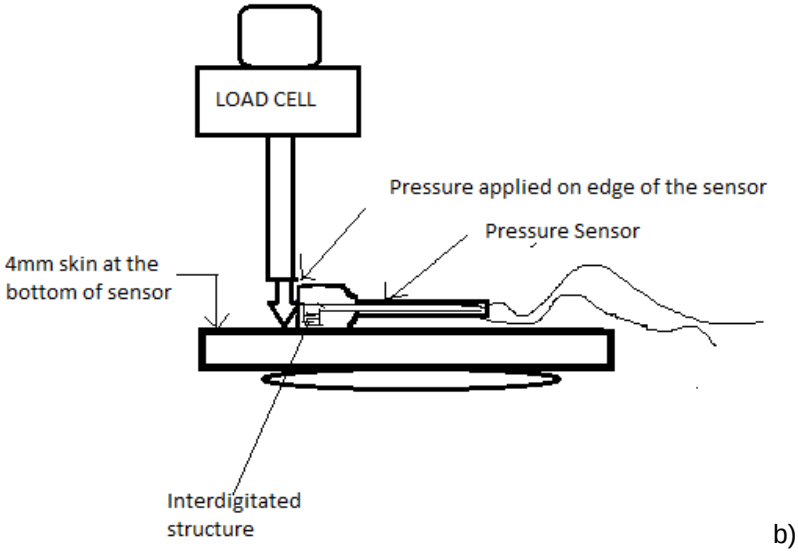

b)

Figure 16 – a) Application of force on top of the sensor, b) Application of force on the edge of the sensor

Figure 16 b) shows the second method to apply the force. In this method, the force applied is on the outer edge of the sensor module. The pressure sensor has an interdigitated structure just like a strain gauge module. When the pressure is applied on the outer edge of the sensor module or just outside of the sensor module, the

interdigitated structure of the sensor expands due to which the sensor resistance increases. This increase in sensor resistance results in decrease corresponding sensed output voltage. The results obtained using both the methods and their differences are shown in further part of this thesis report.

3.1.2 PCB design and development for sensor interfacing circuit

Newly designed and fabricated high resolution pressure sensors are going to be integrated on the robot skin. This will take the physical Human robot interaction to a new level. In order to read the data from these high resolution pressure sensors, some sensor integration circuitry is required. When the pressure is applied, the range of resistance change for these pressure sensors is very small. So it is necessary to have some provision to measure the unknown resistance of few ohms or could be milliohms. For this purpose, the circuit is developed which consists of the Wheatstone bridge along with an operational amplifier (Op-amp).

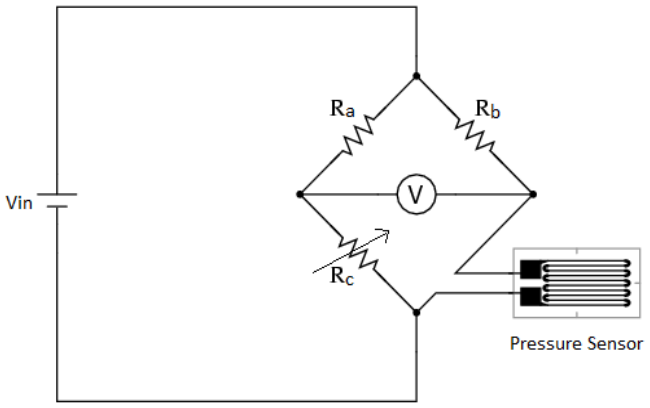

Figure 17 – Wheatstone bridge circuit

The Wheatstone bridge is the circuit which uses the combination of two series-parallel structures of the resistances. These structures are connected between the ground and voltage supply. The Wheatstone bridge circuit has two input and two output terminals which is shown in Figure 17. When the bridge is balanced, the parallel

resistance structures produce zero voltage difference between two parallel branches. It is an unbalanced circuit where Ra and Rb are the fixed resistors, at one leg, the pressure sensor is attached and Rc is the variable resistor used to match the resistance with the resistance of the sensor. When these resistances are matched, the circuit is said to be the balanced circuit.

To amplify the output response from the Wheatstone bridge, Analog Devices AD623 Instrumentation amplifier is used in the circuitry. AD623 is a high performance single/dual supply operation amplifier having the gain range from 1 to 1000 [42]. The main structure of Sensor interfacing circuit is illustrated in Figure 18.

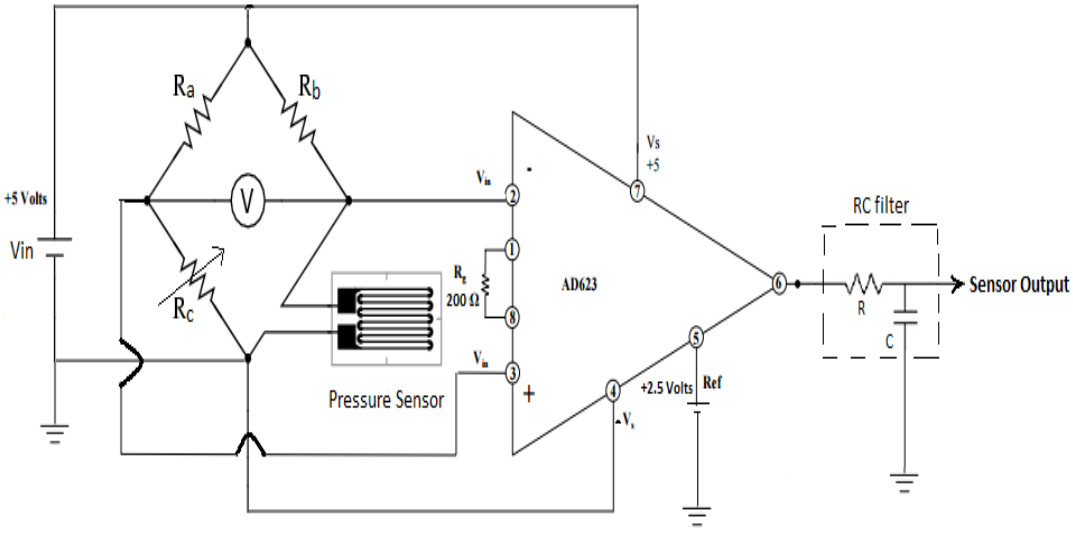

Figure 18 – Circuit diagram for Sensor interface

To measure the smallest change in resistance of the pressure sensor after the application of pressure, a procedure is followed. Initially, the resistance of Rc is matched with the resistance of the sensor to balance the Wheatstone bridge circuit. The Rg resistance of AD623 is provided to set the gain. For this project, the gain chosen is 500. As per the data sheet of AD623 [42], we obtain 500 gain after setting up the Rg = 200 ohms. The 5 volts supply is provided to the supply pins of both the Wheatstone bridge

and the AD623 Op-amp. Pin No. 5 of AD623 is provided to set the reference voltage. We can set any reference voltage from 0 to +5 volts. Here, reference voltage of +2.5 volts is set before performing each experiment. After doing these initial settings, experiments can be performed on the pressure sensors by applying the pressure on them. Depending upon the loading profile, the resistance of the sensor will either increase or decrease and the corresponding change in voltage can be observed. The output of Op-amp is then passed through the RC filter or Low pass filter circuit. This filter helps eliminating any high frequency components or noise. After passing through filter, we can measure the sensor output voltage, which upon applying the pressure on the sensor, either increases or decreases depending on the loading profile as discussed previously.

3.1.3 Experimental Setup for EHD Printing

The separate experimental setup has been used to perform the printing process on the sensors. The Electrohydrodynamic (EHD) inkjet printing method is used for printing the newly developed pressure sensors. It is one of the promising methods of modern inkjet printing as we can print micron sized sensors with variety of features under just one fabrication platform. The hardware setup involves different components, devices and parameters which are discussed further in detail. The EHD printing procedure can be further divided into two parts as – 1) Ink preparation parameters 2) Primary setup for EHD printing.

3.1.3.1 Ink Preparation parameters

The pressure sensors were manufactured using micro-structuring technology. The Poly (3, 4-ethylenedioxythiophene) : Polystyrene sulfonate i.e. PEDOT:PSS is used as a pressure sensing material on the sensors. The cationic charge of PEDOT was balanced by adding the PSS to make the water soluble polymer PEDOT:PSS [43].The PEDOT:PSS is sticky jelly like material, dissolvable in water or other solvents. Two types

of inks were prepared with two different solvents - NMP (1-Methyl-2-pyrrolidinone) and DMSO (Dimethyl Sulfoxide) .These solvents when mixed with PEDOT: PSS produce two separate inks. PEDOT: PSS and DMSO were mixed in the ratio 1:3 to produce one ink and PEDOT: PSS and NMP was mixed in the ratio 1:2 to produce the second ink type.


(a)

(c)

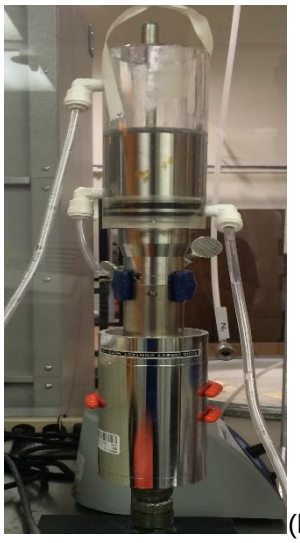
(b)

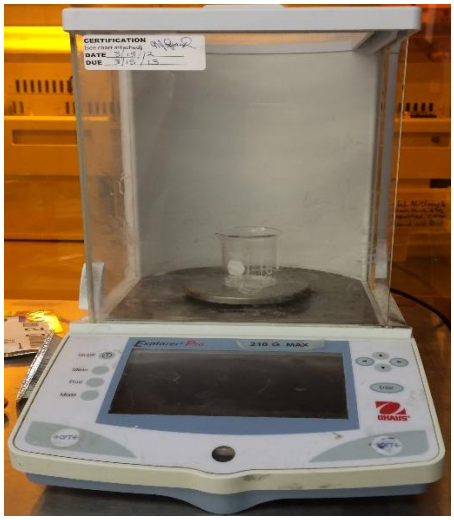

(d)

Figure 19 – (a) Syringe loaded with PEDOT: PSS, (b) Front panel of Sonicator, (c) Sonicator, (d) Weighing machine for ink solvents and PEDOT: PSS.

The equipment used for ink preparation is shown in Figure 19. PEDOT: PSS is first stored in a syringe (shown in Figure 19 (a)). The Ohaus weighing machine (shown in Figure 19(d)) is zeroed every time when we weigh new material. Every time the ink is

prepared, as per the requirement of ink, PEDOT: PSS is pushed out of the syringe and collected in a tube and weighted in Ohaus weight machine. This is the convenient way to use the PEDOT: PSS as it can be precisely used by weight to prepare the ink. After this, the weight machine count is zeroed again and either NMP or DMSO is added to the tube to mix it with the PEDOT: PSS to prepare the ink.

After preparing the ink, it is advisable to sonicate it every time before using it for printing. The sonification process helps remove/dissolve any solvent particles remain in the ink. Figure 19 (b) shows the sonifier used for sonication process. It has one inlet and an outlet. After switching it ON, the tube containing the ink is placed inside the sonicator. The ice chilled water is filled inside the sonicator from its bottom end using the pump attached to the bucket or container and simultaneously an outlet pipe connected at the top side of sonicator, drains the water at the same flow rate as inlet in order to maintain the water level in the sonicator. It is important to note that the water used for the sonication process should be ice chilled water in order to maintain the temperature. Figure 19 (c) shows the front panel of the sonicator. The timer knob at front panel is used to set the time (seconds) of the sonication process. For this project, the ink sonication was done for 15 minutes every time when the ink was used for printing.

There are four printing parameters that need to be fixed: Applied voltage, applied pressure, nozzle travel speed and distance between nozzle and substrate. Wide range of these parameters was used in a trial and error manner to find the optimized parameter for an ink. The parameter optimization was done for two types of ink. PEDOT:PSS with NMP solvent and with DMSO solvent. The ink preparation procedure will be discussed in the next section. A 32 gauge nozzle was used. Agilent 33220A waveform generator is used to generate 1KHz square wave for drop-on-demand inkjet. Trek PM04015A Generator/Amplifier was used as voltage supplier. For pressure control Alicat PCV110

pressure pump was used. It can apply up to 25kPa. A snippet of parameter optimization trial is showed in Table 2 (DMSO) and 3 (NMP).

3.1.3.2 Primary setup for EHD printing

The EHD printing mechanism is advantageous over conventional inkjet printing system for many reasons, one of them is it supports a wide range of materials. It prints with as high viscosity as 1000cP which almost 20 times more than that with conventional printing systems. Figure 20 shows the experimental setup used to perform EHD printing on the pressure sensors.

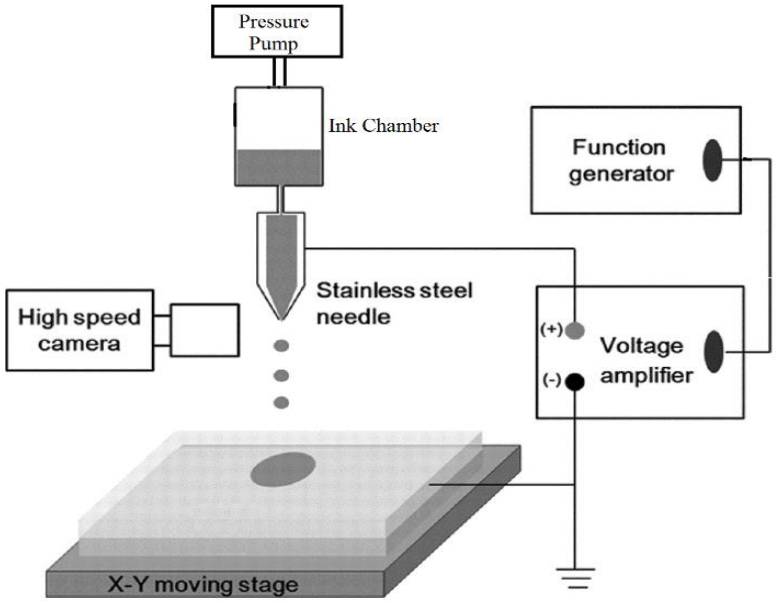

Figure 20 – Experimental setup of EHD printing system

The setup includes various parts, primarily the x-y stage where the sensor is placed for printing. It also has a nozzle to which is the ink is supplied by the ink chamber. The EHD printing method is based on the electric field which is used to pull the liquid out of a nozzle. This Electric field generates the jetting which is smaller than the nozzle size. Pressure is applied to the ink chamber and fluid meniscus is formed at the nozzle tip. The

high voltage supply is connected to the tip and to the substrate, the ground is connected which generates the electric field between the needle tip and the substrate.

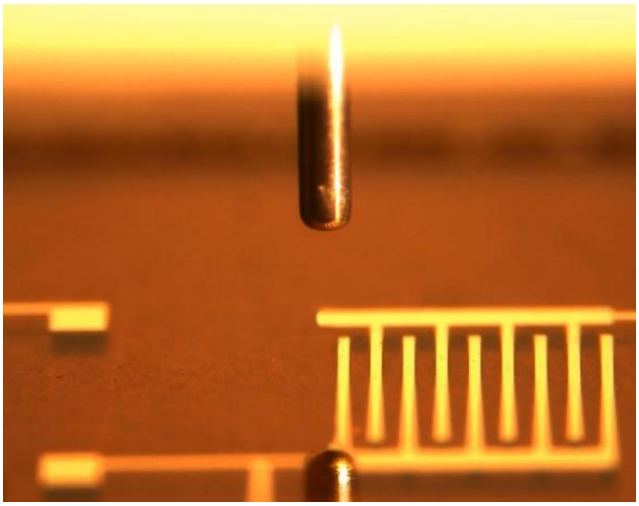

Figure 21 – EHD printing process (Captured by HITACHI CCD Camera)

The system contains the high speed HITACHI CCD camera. It is a high resolution camera which can efficiently record and capture the images even of the micron sized sensors. Aerotech's A3200 Direct Drive system is to control the XYZ stage used for EHD printing. This drive system is primarily based on two communication interfaces – Profinet and EtherCAT. Also, The Aerotech system can control up to 32 axes with high resolution for microfabrication. A 32 gauge nozzle was used for all EHD printing experiments. Agilent 33220A function generator is used to generate 1KHz square wave for drop-on-demand inkjet. Trek PM04015A Generator/Amplifier was used as voltage supplier. As shown in experimental setup, the pressure supplied to the needle by Alicat PCV110 pressure pump. This pressure device can provide up to 25kPa pressure. The software part has been done using LabVIEW software which is discussed in next section.

3.2 Software Development

After setting up the hardware, the major task was to develop the dedicated software for it. The main controller used to control the hardware testing setup is National Instrument's cRIO. cRIO has an ability to accommodate 8 FPGA hot-swappable modules which make it easier to reconfigure cRIO. LabVIEW graphical programming language can be used to program and control cRIO. LabVIEW is used not only to take the measurements but also to observe the corresponding real time waveforms.

3.2.1 LabVIEW Programming for Motion Control

The motion profiles of the hardware components are controlled using motion control software modules. For this project the cRIO uses NI SoftMotion module for motion control applications. As discussed earlier, NI 9516 servo drive interface module is placed on the cRIO chassis. This drive communicates with servo amplifier to acquire the position feedback from the linear actuator which helps performing the position control of the actuator. For tasks such as even handling, trajectory generation and system initialization, SoftMotion programming interface is used.

Many LabVIEW programs, also called as LabVIEW Virtual Instruments (VIs), were created to perform the motion control tasks. After creating a new LabVIEW project, the NI SoftMotion axis was bound to the C series modules used and added to the project. The linear actuator movement depends on the command we provide using the LabVIEW VI. To move the actuator in straight line, the Straight Line Move function block (FB) is used. Figure 22 shows the Straight Line Move FB. This FB is used to perform different moves such as single step, stair step and continuous motion in forward or backward direction. It uses the values specified for total position to be moved, velocity, acceleration and deceleration to move the actuator.

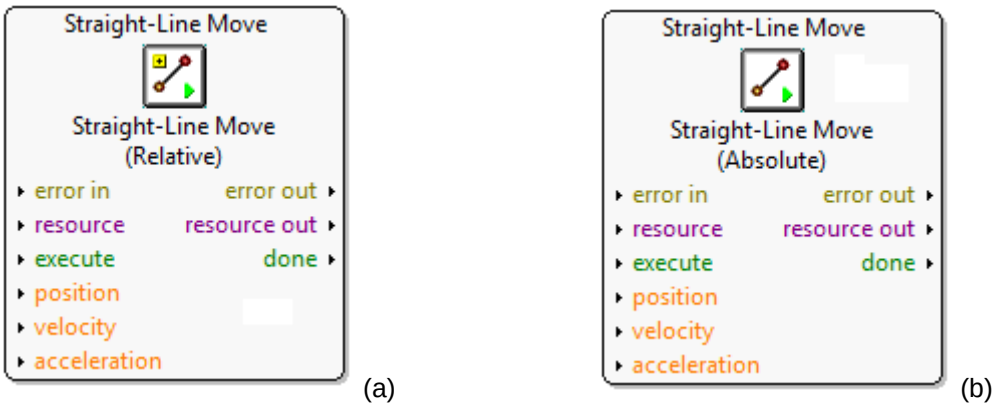

Figure 22 –a) Straight Line FB (Relative), b) Straight Line FB (Absolute)

Two different straight line moves function blocks were used – relative and absolute. The Relative Straight line FB performs the straight line move by locating the target or desired position with respect to the current position at the time when the operation starts. The Absolute Straight Line move FB moves the actuator to the desired or target position with respect to the origin or zero position. The position of actuator origin can be manually set using Axis manager located in the LabVIEW project created. Both FB solve the purpose of straight line movement but with different motion profiles which are discussed in further part of this report.

3.2.2 LabVIEW programs for automated sensor testing and data collection

In earlier sections, we saw how setup was created to carry out the testing on pressure sensors. In this part, the software side of the testing procedure is discussed. All the software programs were developed using LabVIEW. To understand the behavior of newly developed sensors, different tests with different parameter consideration were planned to implement. The experiments were performed based on 6 different parameters, viz. –Ink material used, skin type, motion type –either sinusoidal or square wave, amount of force applied, frequency of applied force and duration for which force was applied. As there are many parameters to be considered for testing for multiple sensors, it makes

difficult to control these tasks manually. Therefore, the automation has been done for all the testing experiments to be carried out which makes the process easier and time efficient. Figure 23 shows the flow chart of test parameters that are automated using LabVIEW.

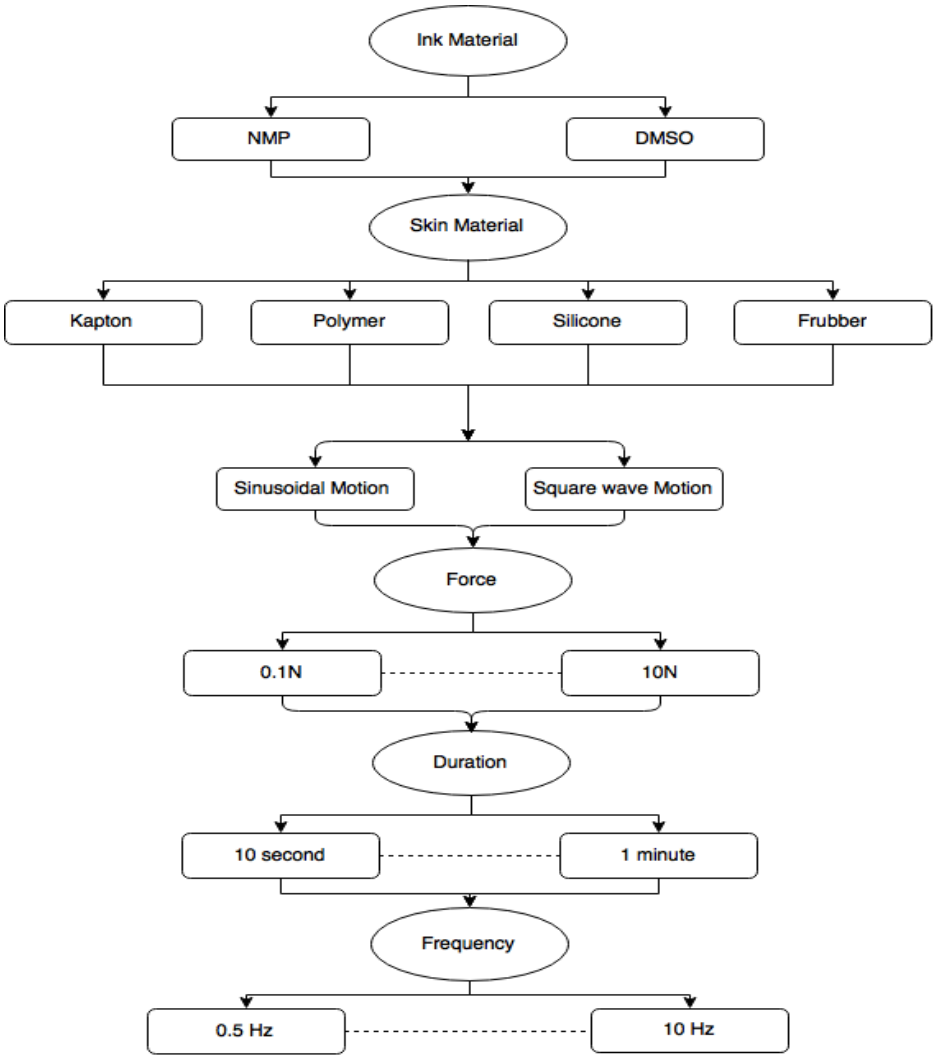

Figure 23 – Flow chart of Automated Test parameters

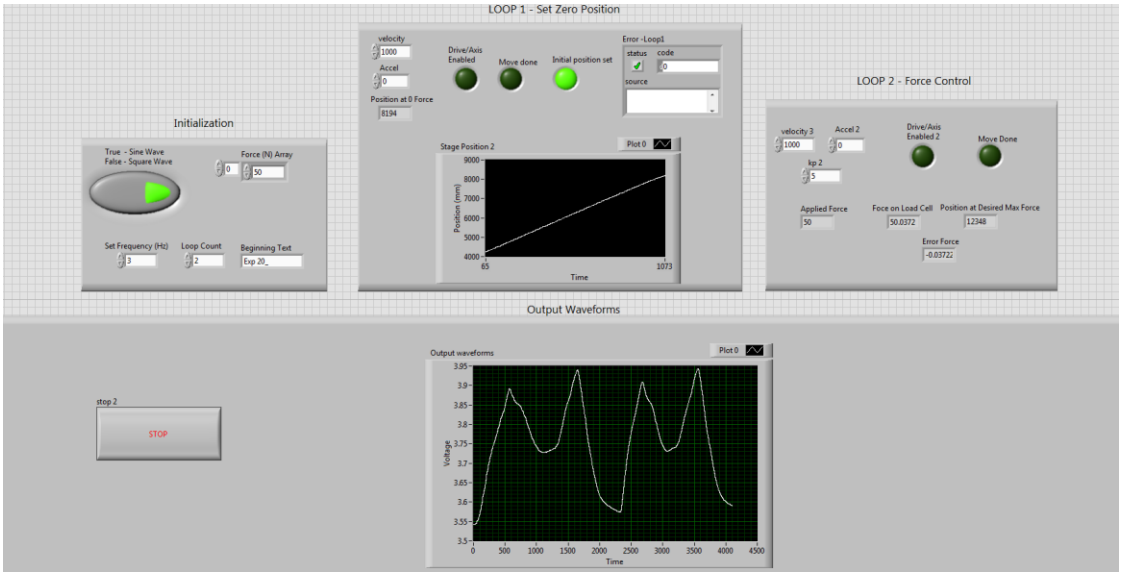

Figure 24 – Front panel of Automated testing VI

Different loops were created in LabVIEW under just one VI in order to automate the whole process. The simplified front panel of automated testing VI is shown in Figure 24. This VI allows to set and control all the parameters required to perform testing on the sensors, as mentioned in the flowchart. On the left hand side of the front panel, the parameters are initialized which includes – Selection of sinusoidal or square wave motion, range of forces to be applied, range of frequencies to be applied, number of counts to repeat the sinusoidal or square wave motion and the current experiment number in order to save it in the csv file. These parameters are set before running the VI. Once the run button is clicked, the set of experiments start as per the initialization parameters. The middle block shows the real time waveforms of position change of the actuator and the waveforms at the bottom gives the motion profile applied on the pressure sensors in real time. Figure 25 shows the snippet of Sinusoidal motion block and Figure 26 shows the snippet of square wave motion block. At first, each time before starting the sinusoidal or square wave motion, the plunger position is marked when the

plunger just touches the sensor i.e. at zero force value and also the final position for the maximum force set to be applied i.e. the maximum force position. Once the positions are set, the sinusoidal or square wave motions are performed automatically without the user prompting. The experiments performed and the respective test results and waveforms will be discussed in the next chapter.

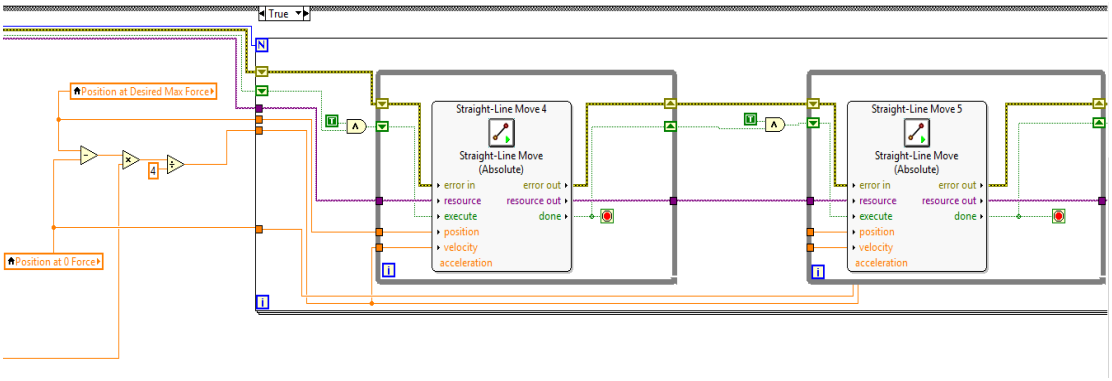

Figure 25 – Snippet of Sinusoidal motion VI

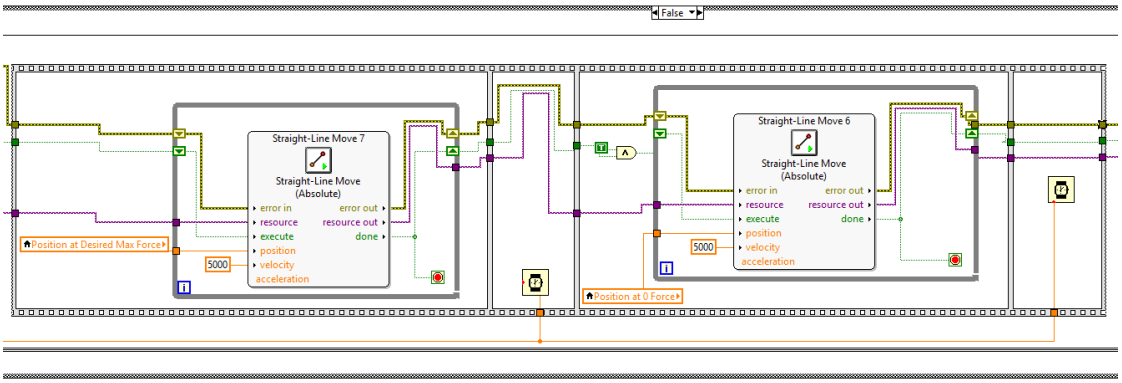

Figure 26 – Snippet of Square wave motion VI

After performing the required set of experiments, the tough part was to save all the data in the designated file depending upon the parameters used for the experiments. It is very difficult to save all the files manually as there could around 180 files in total for a single

sensor, considering all the parameters used for testing. So it necessitates to automate the whole file saving process to make it easier and time efficient. Previously, the experiment files were used to save in the cRIO memory. But, the cRIO offers only a few megabytes of memory which is insufficient to save all the test data. The file saving process was divided in two VIs – some part in main testing VI and then most of the part in separate file saving VI. The reason why this process is divided into two parts is to synchronize the cRIO with PC. The file saving VI is written is such a way that it will store the data collected from the experiments directly into the computer. This will not only save the time to store the data but also alleviates the problem of memory shortage which was in the case of cRIO. Figure 27 shows the snippet of file saving VI.

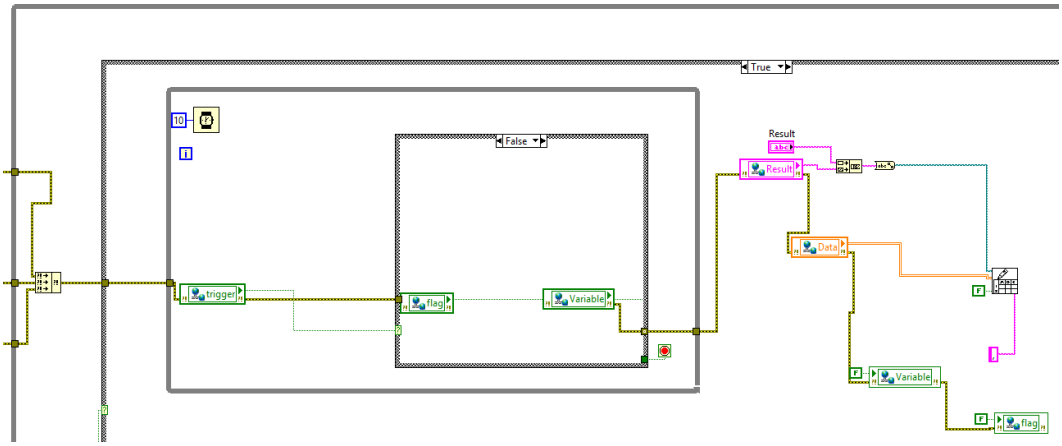

Figure 27 – Snippet of File Saving VI

As can be seen from the above figure, many shared and local variables are used in the file saving VI. These variables are nothing but the data storing and transferring variables just like the variables used in other programming languages such as C programming. The local variables can only be used in the same VI or program file whereas the shared variable can be used in same as well as different VI. These variables are particularly used in order to have synchronization between main testing VI and the file saving VI.

When the testing is done, the data get stored in the shared variables. The same variables are also used in the file saving VI so that the data stored in those variable can be stored in the file. The file path VI in the program helps storing the array of strings or data collected from measurements in the each individual file for each experiment performed. Every program or VI has the dedicated Stop button. When the stop button is pressed, the array consisting of the acquired data is stored into a tab-delimited file. This file is then sent to the file path specified in the file path VI or block.

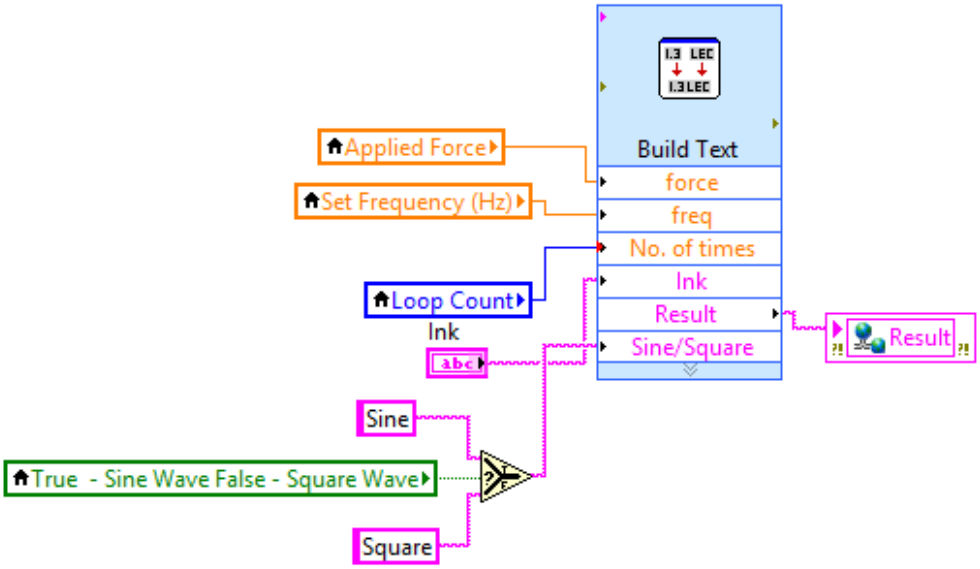

Figure 28 – File name created using shared variable

The example how of the file name is created dynamically is shown in Figure 28. All the parameters are inserted into one VI which builds the text and creates the string at the output. This string is then stored in a shared variable which can be accessed in the same or the other VI. This snippet was created in main testing VI. After executing the main testing VI, the control is automatically transferred to the file saving VI where this 'Result' shared variable is used in order to provide the data collected to the file saving block.

3.2.3 Implementation of Force Control Schemes

The term force control implies the property of modification or changes in the position of the robot based on the applied force. For many industry applications, controlling the robots in contact with the environment is a difficult task. Controlling the physical contact between the robot and the environment is a primary requirement for the success of a manipulation of the model.

Different control schemes were created using LabVIEW and applied on the sensors. At first, position based force control was tested. For that Incremental force control scheme was executed on the sensors. Figure 29 shows the block of Incremental force controller VI. In an incremental force controller, the desired force is compared with the force measured by the load cell. The comparison of desired and measured force gives an error force value.

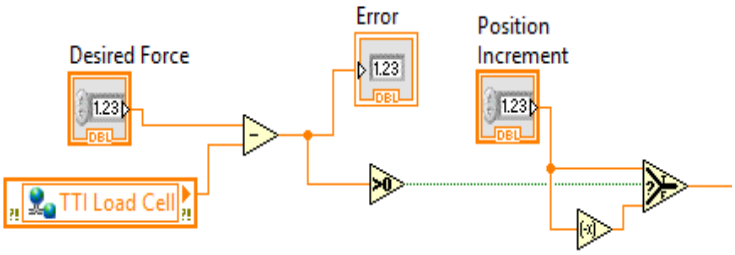

Figure 29 – Incremental force control

The comparison of desired and measured force gives an error force value.

$$e_f = f_d - f_a$$

Where,

e_f = Error force

f_d = Desired force

f_a = Applied force

The experimental results obtained for the incremental force controller are shown in Figure 30. In that, the red curve indicates the force applied on the flexi force sensor and the white curve represents the desired force needed. We can clearly see that, the response of this controller is very slow as the applied force takes time to reach to the desired value. This is the main disadvantage of the Incremental force control. To overcome this we need an explicit force control scheme.

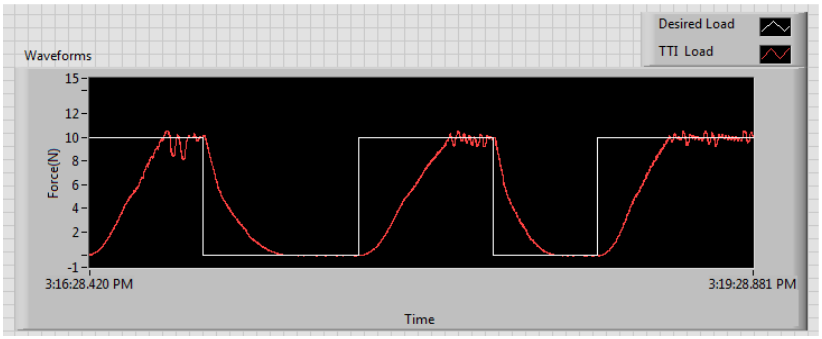

Figure 30 – Real time waveforms for Incremental force control

To overcome the problem of incremental force control, explicit force control was developed. It is the most basic active force control algorithm. Figure 31 shows the basic structure of an explicit force control scheme. This controller takes the direct commands measurements of the force values.

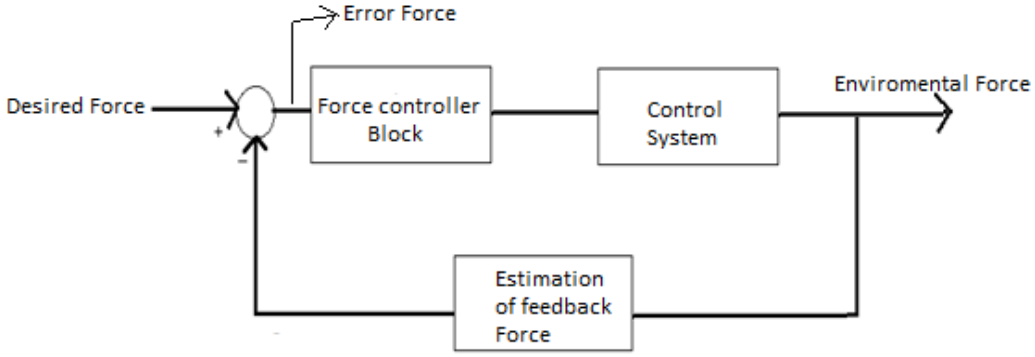

Figure 31 – Block diagram of explicit force control scheme

In this the desired and measured force are compared with each other and an error signal is fed to the controller which processes it. After this, the processed signal is fed directly to the control system. We can implement such control scheme with any controller like P, PI, PD or PID. Here, we have used the PD controller. The dynamic equation of the system is given as [44] –

$$x_s = k_p(f_d - f_e) - k_d f_e$$

Where,

x_s = actual position of the actuator

k_p = proportional gain

f_d = desired force

f_e = environmental force

k_d = derivative gain

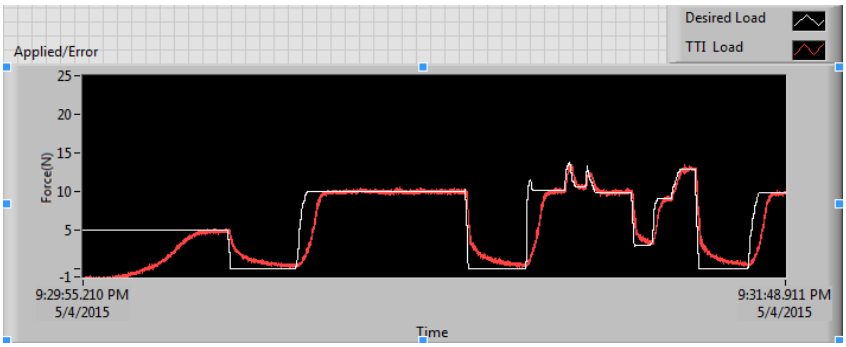

Figure 32 - Real time waveforms for explicit force control

The experiments for force control scheme were performed on two different skin samples of different stiffness vs. Frubber skin andP10 silicon polymer skin. The Frubber skin is softer than P10 polymer. Figure 10 a) and 10 b) shows the responses obtained with P10 polymer skin sample. The P10 skin material is quite hard and stiffer than Frubber skin. Therefore, when the experiments were performed with both the skins, we

got much smoother and faster response using P10 polymer skin. The actual force (red waveforms) catches up faster with the desired force value. Also, the sensed force is monitored. When the same 10N force is applied, the measured force observed was around 4 N with Frubber sample and around 7N with P10 sample. This is because of the thick and stiff nature of P10 silicon. So we can clearly see that, the explicit force control scheme is more effective than the incremental force controller in all the considered aspects. The explicit force control also has some disadvantages. The main disadvantage of an explicit force control is that, it chatters when the robot comes in contact with the environment. Also it provides poor disturbance rejection. These drawbacks lead to the development of an Impedance control scheme.

The primary objective of an impedance control strategy is to control the target impedance which is nothing but to develop a desired dynamic relationship specified by the user. The mechanical impedance is nothing but the relationship between the input velocity and the applied force. In this, the forces are indirectly applied since the primary control mechanism is based on the position error between the actual position of the actuator and the desired position to be achieved. Here, the forces are only indirectly assigned by controlling the position unlike the explicit force control. Trade-off between contact forces and position accuracy occur due to a certain stiffness in the impedance model along a Cartesian direction. To implement this technique, we can model it through a generalized dynamic impedance, which is a complete set of mass-spring-damper equations. The equation can be modeled as follows

$$f_a = \left(d_a - \left(\frac{m_a}{m_d}\right) d_d\right) \dot{x} + \left(k_a - \left(\frac{m_a}{m_d}\right) k_d\right) x + \left(1 - \left(\frac{m_a}{m_d}\right)\right) f_s + \left(\frac{m_a}{m_d}\right) (d_d x_d + k_d x_d)$$

m_a, k_a and d_a represent actual mass, spring and damper of manipulator and m_d, k_d, d_d are the mass, spring and damper of the desired environment. Actual force or the applied force is represented as f_a whereas f_s is the feedback or sensed force.

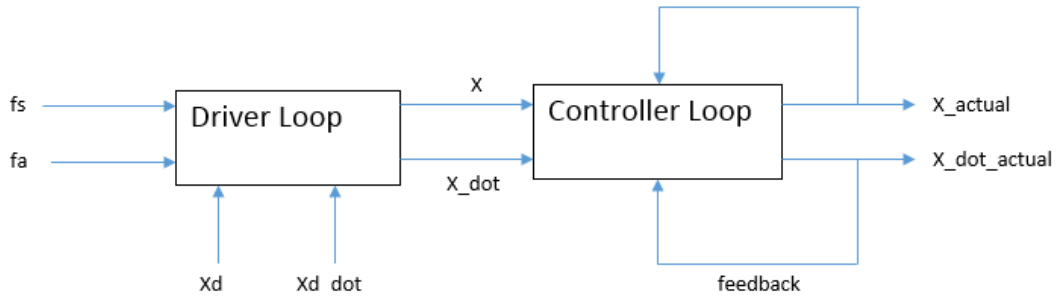

Figure 33 – Block diagram of Impedance control scheme

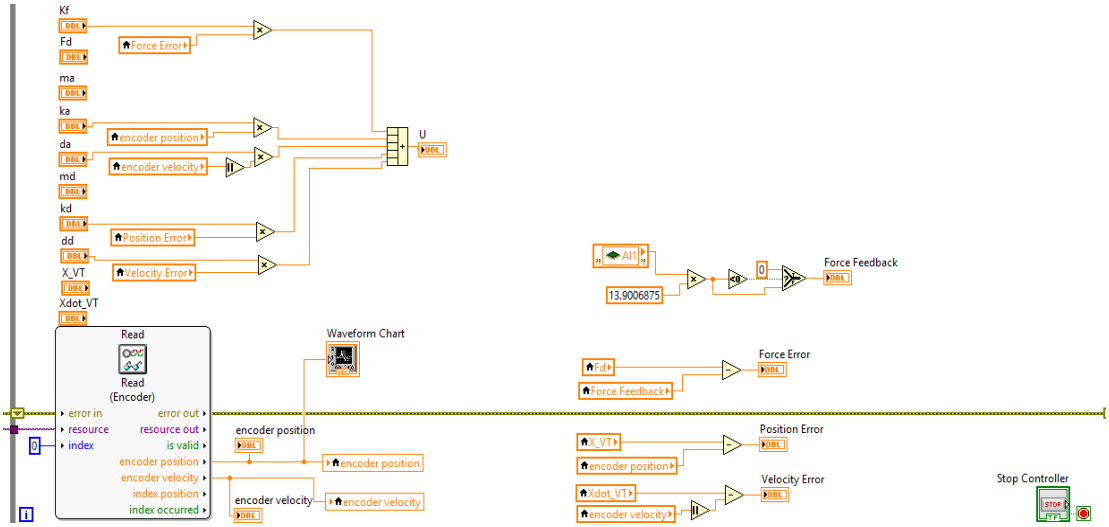

Figure 34 – Impedance control VI

The block diagram of Impedance control developed for this project is shown in Figure 33. As can be seen, the process involves two loops viz. Control loop and driver loop. Initially in driver loop, the desired trajectories for position and velocity are generated using mass spring damper parameters of both the manipulator and model/sensor. Also, the applied and sensed force are taken into the consideration and used to drive the loop.

The trajectories from the driver loop are then fed to controller loop. This loop drives the motor and hence the manipulator. With each movement of manipulator, the position and velocity trajectories tracked by the controller are fed back to the control loop. The manipulator continues to move until the desired trajectory is reached. Figure 34 shows the snippet of the LabVIEW program developed for Impedance control scheme. An impedance control technique maintains a strong contact interaction between the robot and the sensors so that it will not damage the sensors.

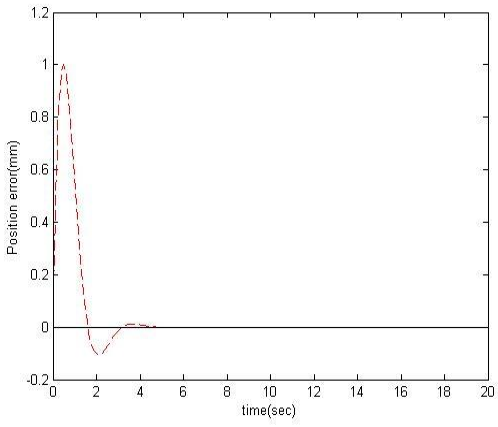

(a)

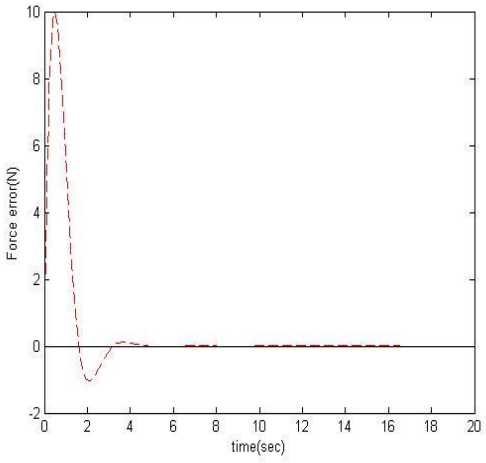

(b)

Figure 35 – a) Position error (mm) with c_d = 14, b) Force error (N) with c_d = 14

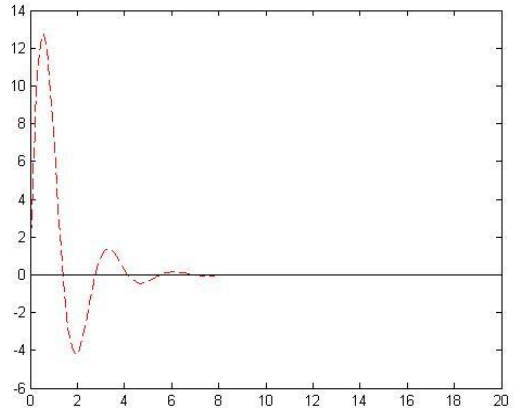

(a)

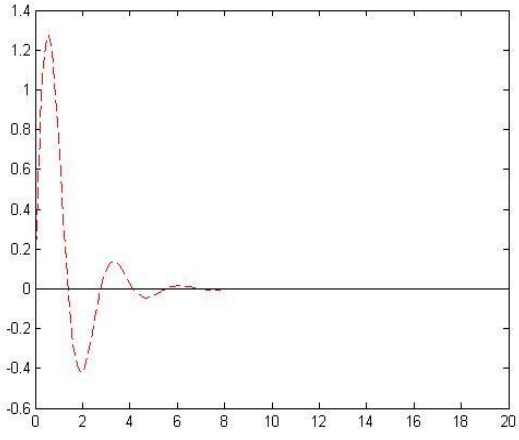

(b)

Figure 36 - a) Position error (mm) with c_d = 8, b) Force error (N) with c_d = 8

First, the simulation tests for Impedance control scheme were performed using MATLAB. These results were obtained for various combinations of values of the mass spring and damper constants of the system, environment and the impedance model. The simulation results shown here are obtained for two different damping constants of impedance model as c_d = 8 and c_d =14 by keeping the other parameters same as:

m_a = 0.5, c_a = 0.8, k_a = 0.2, m_d= 5, k_d = 10

Where, m_d, k_d and c_d are the mass spring and damper constants of the impedance model used for the simulation purpose.

The simulation results obtained for impedance control are shown in Figure 35 a), b) and Figure 36 a) and b). Here we observed the error values of desired and actual position and the desired and actual force. The results were obtained for different parameter values. The output responses with different damping constants are shown here.

Figure 35 a) and b) are the results with damping constant c_d = 14, whereas, Figure 36are results with c_d = 8. We can clearly distinguish that if the damping constant is higher, by keeping the other parameters unchanged, the error values of position and force quickly converges to zero. With c_d = 8, we get more oscillations than that with c_d =14.

In order to apply constant, desirable force on the sensors, we used an explicit force control technique. Use of an explicit force control scheme might result in problem of chattering and unstable response in some case, which led to the development of an impedance control technique. For this particular project, we were applying force on sensors which were placed on top and/or underneath the soft skin patches. For this thesis, we have used skin materials which are quite softer and flexible in nature, which minimizes the possible chattering effect even if an explicit force control is applied. Due to this fact, we deiced to continue the use of an explicit force control

Chapter 4

Experimental Characterization of EHD printed Pressure Sensors

4.1 Pressure Sensors

The pressure sensors used for this project were fabricated at University of Texas at Arlington. These pressure sensors has an Interdigitated structures patterned on the Kapton substrate. Various shapes can be patterned on the Kapton substrate for the sensors. The two electrode patterns that are being used for the piezoresistive sensors are shown in Figure 37.

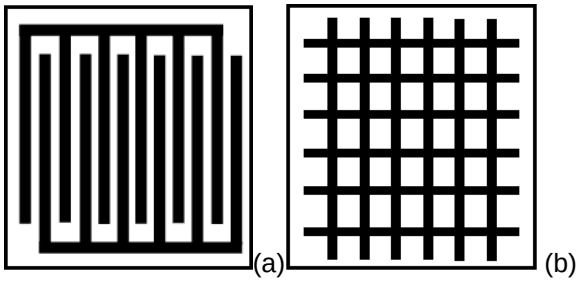

Figure 37 – Electrode patterns: a) IDE Structure, b) CPE Structure

Figure 37 a) shows an Interdigitated Electrode Structure (IDE) and Figure 37 b) shows the structure of Cross-point electrode (CPE). In Cross Point Electrode, the sensing area is sandwiched between two neighboring electrodes. The IDE structures can be fabricated at Nano scale. These structures are commonly preferred in MEMS applications. For this project, pressures sensors were fabricated in Interdigitated Electrode structure (IDE). These sensors were patterned on the Kapton substrate. The snapshot of the Single pressure sensor module is shown in Figure 38. We can clearly see the Interdigitated Electrode structure (IDE) on the left hand side of the Figure 38. A piezoresistive material PEDOT: PSS was layered on an interdigitated structure due to which sensors reflects the piezoresistive material properties.

Pressure sensors can be characterized using different methodologies. To perform testing operations, the specific set had been created. The setup consists of Pressure sensors, a Load cell to apply the force on the sensors, Frubber and P10 silicon polymer skins to place at the bottom and top of the pressure sensor and controller and driver hardware to collect the experimental data in real time.

Figure 38 – Single Pressure Sensor module

Figure 39 shows how an interdigitated structure exhibits its properties. When the force is applied on the top of the senor, an interdigitated structure of sensor compresses and it will result in decreasing resistance properties. In contradiction to this, if the force is applied anywhere outside or on the outer edge of the sensor, an interdigitated structure of sensor expands which results in increasing resistance of the sensor module.

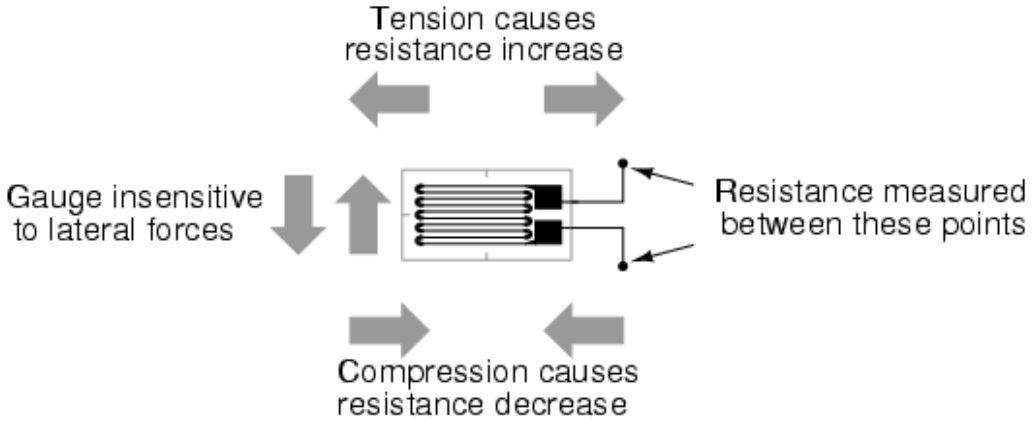

Figure 39 – Working of an Interdigitated Electrode Structure [45]

For this thesis, EHD printing had been done on 6 different sensors. The number of layers of ink material used while EHD printing were different for all six pressure sensors. Based on the ink material used and the number of EHD printing layers applied on each sensor, six sensors can be classified as shown in Figure 40. The results obtained, after characterizing pressure sensor of different types, will be discussed in the next section of this chapter.

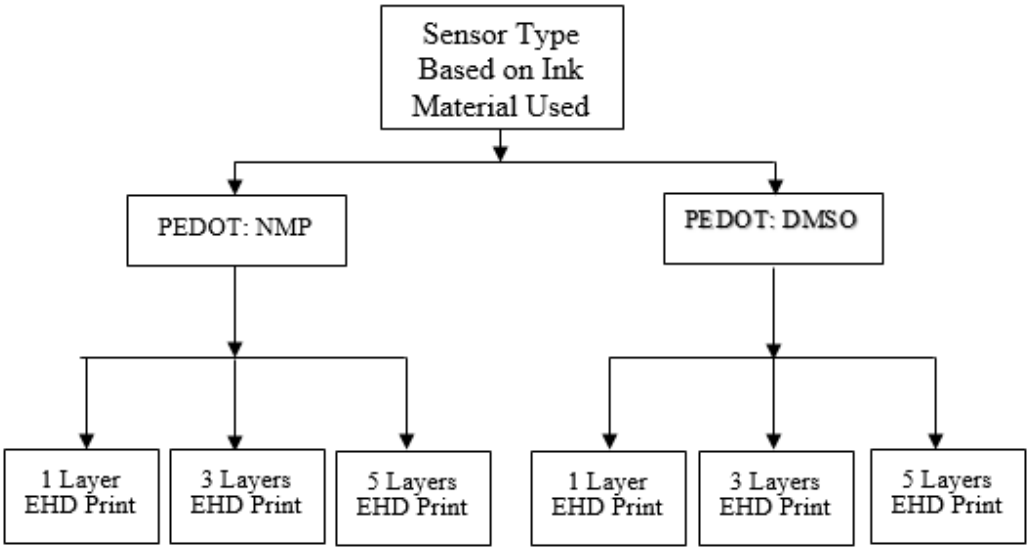

Figure 40 – Classification of Pressure Sensors based on Ink material used for EHD Printing

4.2 Sensor Testing Procedures and Parameters

After setting up the initial hardware and software, various parameters for testing were considered, such as sensor placement, resting resistance of sensors, type of skins to be used, placement of skins related to sensors, hardware tuning and size of load applicator. The effect of each parameter and resulting outcomes from sensors will be discussed in the next section. Two primary testing procedures were followed – 1) Static testing 2) Dynamic testing. The static testing includes an application of stepwise

increasing and decreasing force on pressure sensors. A range of forces, from 1 Newton to 10 Newton, was applied in a stepwise manner and by resting for 10 seconds at each step of force increment or decrement. The dynamic testing was carried out using sinusoidal movement loading profile. Force, ranging from 1 Newton to 10 Newton, was applied with different frequencies of sinusoidal motion. To compare the effect of different frequencies, a minimum of 3Hz and maximum of 10Hz of frequencies were considered.

4.3 Experiments, Challenges and Observations

Previously, the sensors used to be mounted on a flat aluminum stage having no provision to record at what position the sensor was mounted. The drawback of such stage was that, if the sensor was moved from its position during testing, it was almost impossible to remount it at the exact position which is quite obvious as the sensors are very small having an interdigitated structure dimensions of 1.32 mm x 1.32 mm. To understand how sensors react to human like contacts, newly developed 3D printed cylindrical plunger was used to carry out further experimental process. The structure of human finger-like plunger is shown in Figure 41.

Figure 41 – 3D printed finger-like plunger

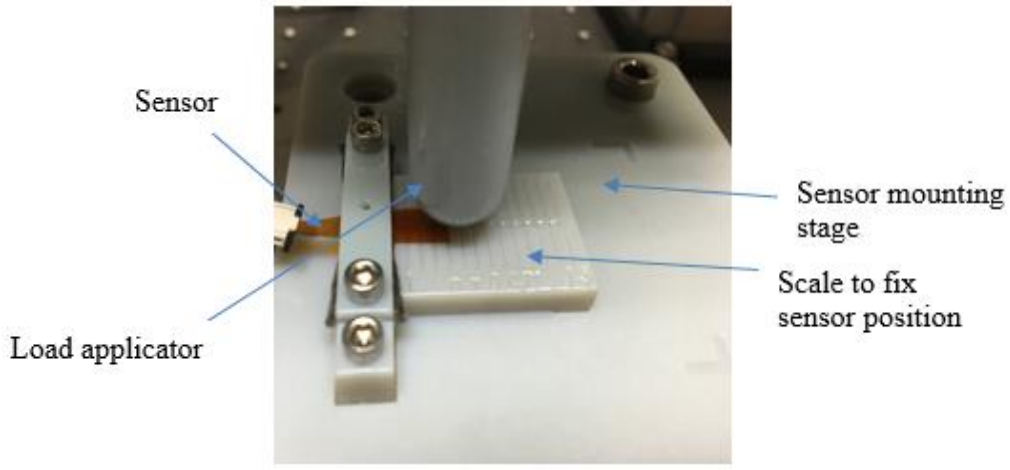

(a)

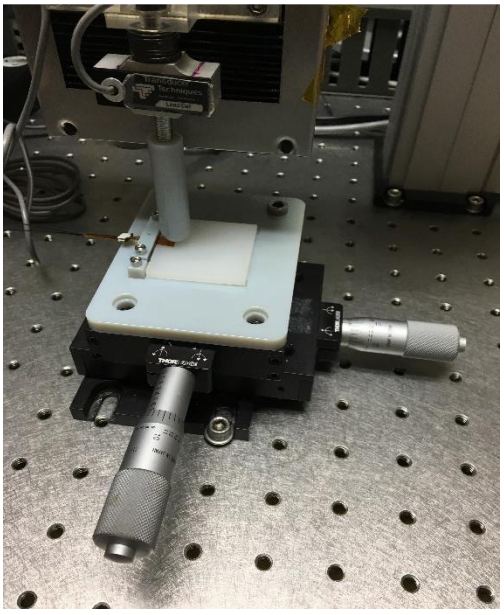

(b)

Figure 42 – a) 3D-Printed test fixture, b) 3D-printed test fixture mounted on X-Y stage

Figure 42 a) and b) shows a 3-D printed test fixture and how it was mounted on X-Y stage, respectively. The scale, used to adjust and fix the sensor position, helps to remount a pressure sensor back to its original position, if moved or removed during the testing process. This alleviates the problem of possible drift in output due to misalignment of sensor mounting. Figure b) shows how a pressure sensor was fixed on a 3D printed

stage which was then mounted on X-Y stage. The X-Y was used to move adjust the sensor position with respect to the position of load applicator. X-Y stage can moved manually using micrometer scale available for both X and Y axes of a stage. These scales help to precisely adjust the sensor position.

Resistance of a pressure sensor to be tested was measured each time before doing any tests on a pressure sensor. After noting down the resistance, we connect the pressure sensor to the Wheatstone bridge circuitry. Depending upon the measured resistance of a pressure sensor, the Wheatstone bridge had to be tuned every time before doing any experiments by varying the value of a potentiometer connected to another leg. This procedure had to be followed in order to tune the circuitry and hence to measure the exact output response from pressure sensors.

For this project, the pressure sensors were packaged with two types of artificial robot skins – Frubber® and P10 silicone polymer skin. The idea was, the pressure sensors will be integrated in the robots covered with the soft skin. Various soft skin materials can be used, but in thesis we have used Frubber® and P10 polymer. After selecting the skins, it was highly important to understand the behavior of each skin type. To understand the properties of both the skins, extensive testing was done on sensors with combinations of two skins above and/or below the sensors. Hysteresis and drifts were experienced with both Frubber® and P10 silicone polymer skin. Drift results due to the fact that the soft skin material relaxes after the application of constant force input. Hysteresis shows the non-linear behavior which occurs when the relationship between system's input and output differs during loading and unloading motion profiles [46]. To understand and observe hysteresis and drift properties, experiments were performed by indenting the plunger into skin and hence applying force on sensors using different motion profiles.

Piezoresistive pressure sensors are very sensitive to the environmental conditions. To have a better understanding of environmental effects, Also, a sensor's response was observed under Thermal Imaging Camera available at University of Texas Arlington Research Institute (UTARI). When a sensor was put near flame and observed under Thermal Imaging Camera, it clearly reflected the temperature effects on the sensor. Simultaneously, the change in resistance was also observed using Digital multimeter. The similar test was done by holding ice instead of flame near the sensor and the change in sensor's response was observed. The room temperature was also tracked for a few days while performing experiments which was in the range of 71° to 75° Fahrenheit, and averaged to 72° Fahrenheit. The drifting problem of pressure sensors can be reduced by reconsidering its material properties. Also, in the future, it would be beneficial to redesign a Whetstone bridge circuitry by adding a Half bridge circuit [47] [48]. In Half bridge configuration, active strain gauges are used in both arms of a Wheatstone bridge. So, any change in temperature affects both strain gauges in a same way. Because the temperature changes are same at both arms of bridge, the ratio of resistance change for two arms do not change which in turn results in no change in output voltage and avoids any drift due to temperature effects [47].

For this thesis, 4mm Frubber®, 4mm and 2mm P10 silicone polymer skins were used for testing and characterization of Electronic skins. These skins can be placed above and/or below senor modules to be tested. The response from skin changes by changing their combinations. To perform experiments, pressure sensors were fixed to a position using scale on a 3D-printed test fixture and X-Y stage's micrometric scale, with different skin combinations above and/or below sensors. A sensor used for this particular experiment was PEDOT: NMP (3 Layers). After gathering the initial set of experiments it was identified based on the data collected, that the sensor placement was not

appropriate. The conclusion was made after carefully observing the waveforms for experiments with same set of parameters and loading profiles. The force was applied on top of the sensor's interdigitated structure. An experimental setup is shown in Figure 43 a). It was identified that the length of sensor tail was too large which caused a sensor to bend from middle in upward direction as shown in Figure 43 b).An example of this inconsistency in sensor's response is depicted in Figure 44.

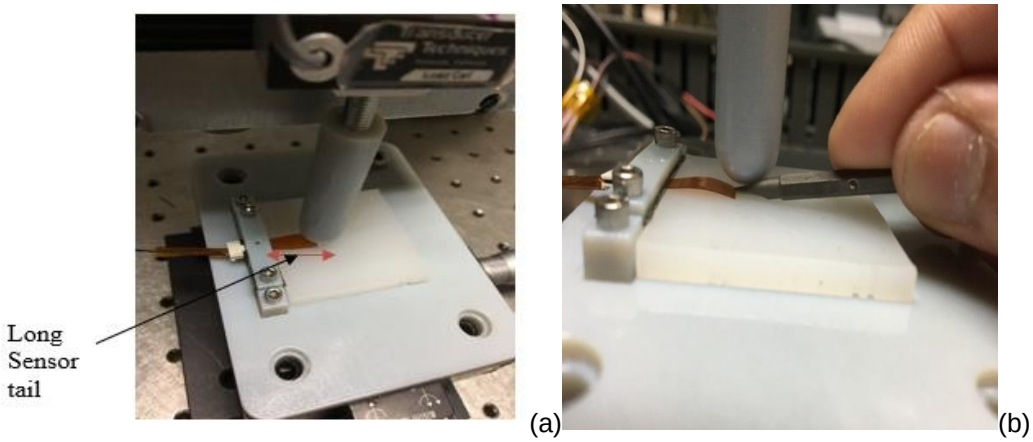

Figure 43 – a) Setup exposing Long Sensor Tail, b) Sensor bends with Long tail

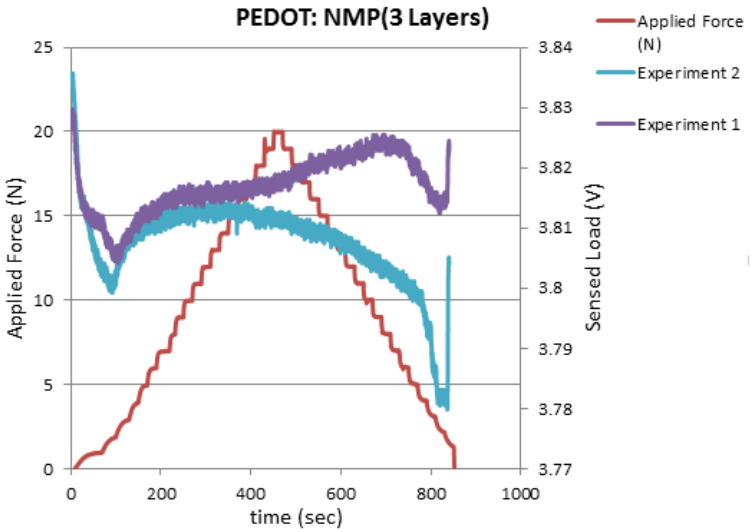

Figure 44 – Inconsistency in Sensor's Response due to Long Sensor Tail

After observing the problem of long sensor tail, the sensor was moved backward and fixed to test fixture by making sure that minimum required sensor part was exposed and placed on the soft skin, in this case 4mm P10 Polymer skin, as shown in Figure 45.

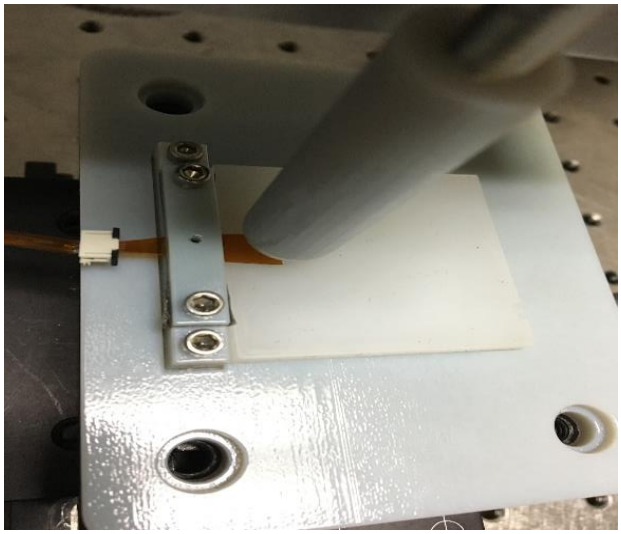

Figure 45 – Setup exposing Short Sensor Tail

Furthermore, the position and placement of sensors on X-Y stage was taken into the consideration. Tests were carried out by applying force at different locations on and near sensor's interdigitated structure. The idea behind this test was to observe if there was any significant change in sensor's response in terms of spatial uniformity and linearity. By varying micrometric scales present at both X and Y stages, sensor's position with respect to plunger was changed. X-Y stage can be moved with a step resolution of 25 microns (0.0254mm). Figure 46 shows how the force was applied at different positions. With respect to sensor's position, force was applied on top of sensor (zone 0) as well on three different directions (zone 1, zone 2 and zone 3) as shown. In each three directions, force was applied uniformly by adjusting the plunger position at three different distances away from sensor. Yellow point indicates an application of force on top of sensor's interdigitated structure while red, blue and green points indicate an application

of forces at a distance of 1.27mm, 2.54mm and 3.81mm, respectively, away from senor's interdigitated structure.

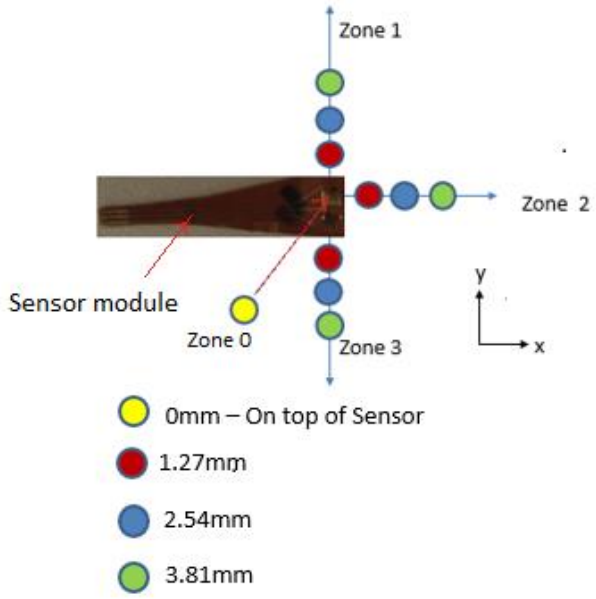

Figure 46 – Force application at different positions

These loading profiles were applied with a combination of different types of sensors and skin materials.

Figure 47 shows an example of output responses from DMSO (5 Layers) sensor after an application of sinusoidal motion profile at different zone positions with respect to sensor module and with 4mm P10 Polymer at bottom and 2mm P10 Polymer skin at top of pressure sensor module. The blue curve represents the applied force trajectory whereas green curve is the sensed output from a sensor module. At first sight, it is easy to differentiate, that the sensor response varies depending upon the position of applied force (10 Newton Max.) in any direction for same loading profile. The reference voltage for each curve is different as it changes over time due some factors such as drift in sensor response due to hardware parameters and change in sensor resistance over time. If we consider the sensed output voltage, that is, the difference between reference

voltage and maximum voltage sensed for each curve, then we can easily differentiate the sensed voltages at different positions.

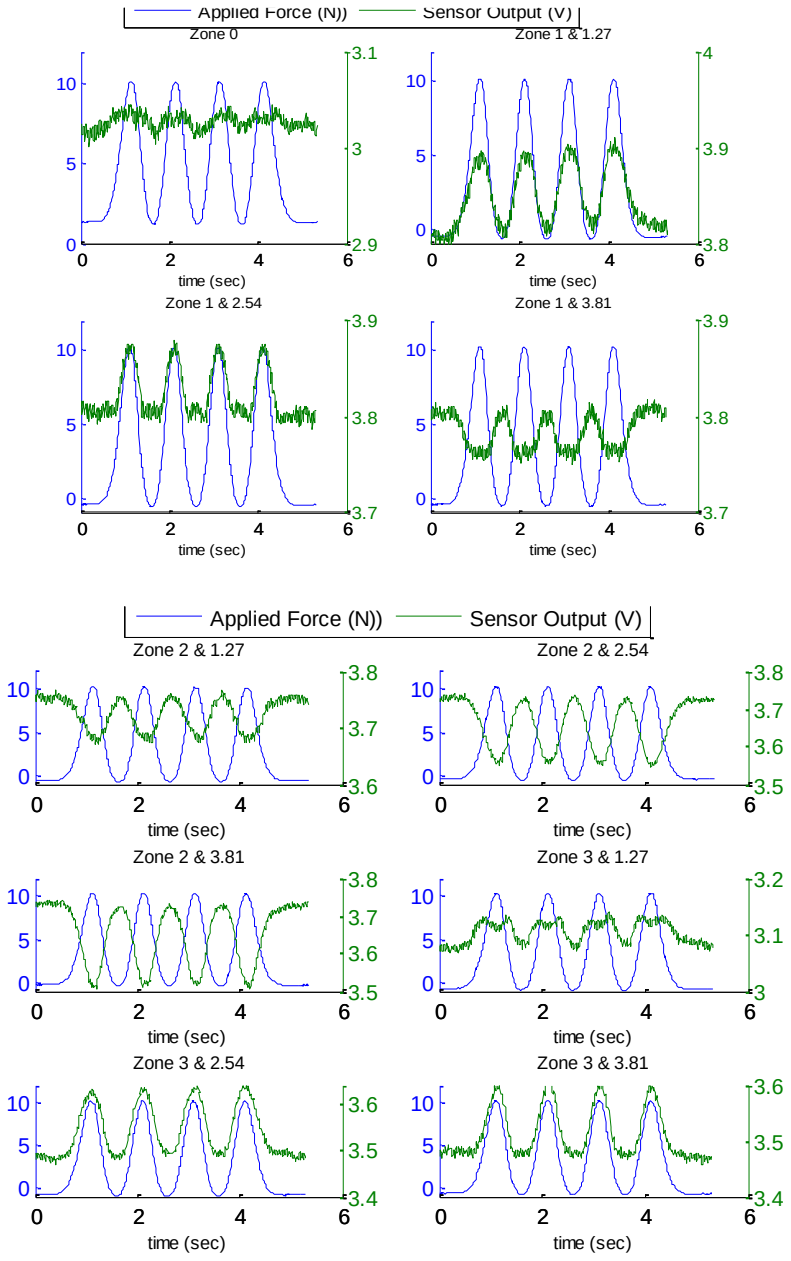

Figure 47 - DMSO (5 Layers) Sensor: Force Application at – a) Zone 0 and Zone 1, b) Zone 2 and Zone 3

As we can see, when force is applied on top of sensor i.e. at zone 0, the sensor output incorporates a lot of noise in it. The sensed voltage at zone 0 is comparatively less than that when force is applied in zone 1, zone 2 and zone 3.

The output voltage trajectories obtained for all the zones are different. It can be seen, that the output voltage trajectory is directly proportional to the applied force trajectory when force is applied in zone 0, zone 1 (except at 3.81mm) and zone 3 because sensor resistance decreases in these regions which in turn causes the output voltage to increase proportionally. In contradiction to this, the output/ trajectory obtained at zone 2 is inversely proportional to applied force trajectory because the sensor resistance increases with increasing applied force which causes an output voltage to decrease proportionally. As per the strain gauge properties, this explains, that the sensor experiences more strain in the direction of zone 2 compared to zone 1 and zone 3 which results in inverse proportion of applied force and output voltage trajectories. Output response at zone 1 slightly degrades as we keep going away from the sensor module. Unlike zone 0, output responses, obtained after applying force at zone 2 and zone 3, improve as we keep increasing the distance away from sensor's interdigitated structure. This is true in case of both smoothness of output voltage trajectory and amount of sensed voltage.

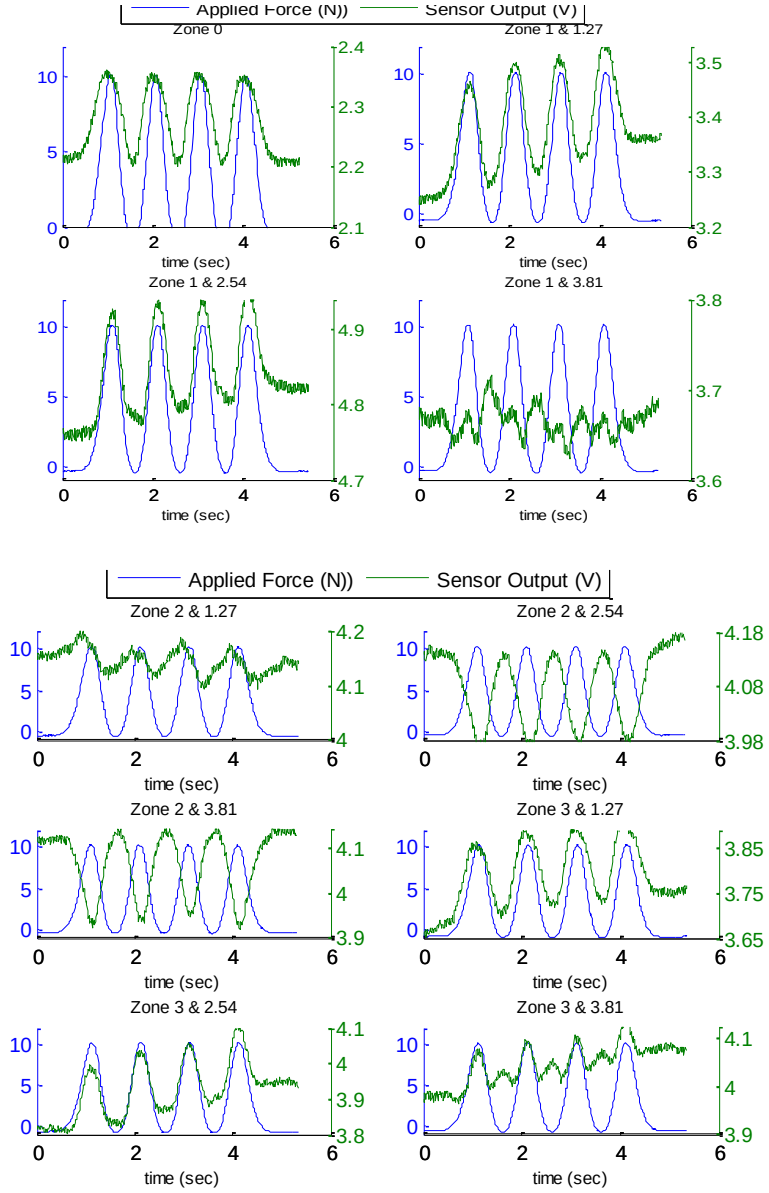

Figure 48 - NMP (5 Layers) Sensor: Force Application at – a) Zone 0 and Zone 1,

b) Zone 2 and Zone 3

Similar curves were plotted for different sensor types with same combination of skins i.e. 4mm P10 Polymer at bottom and 2mm P10 Polymer skin at top of pressure sensor

module. Figure 48, Figure 49 and Figure 50 show the output responses obtained from NMP (5 layers) sensor, NMP (1 layer) sensor and DMSO (3 layers) sensor, respectively.

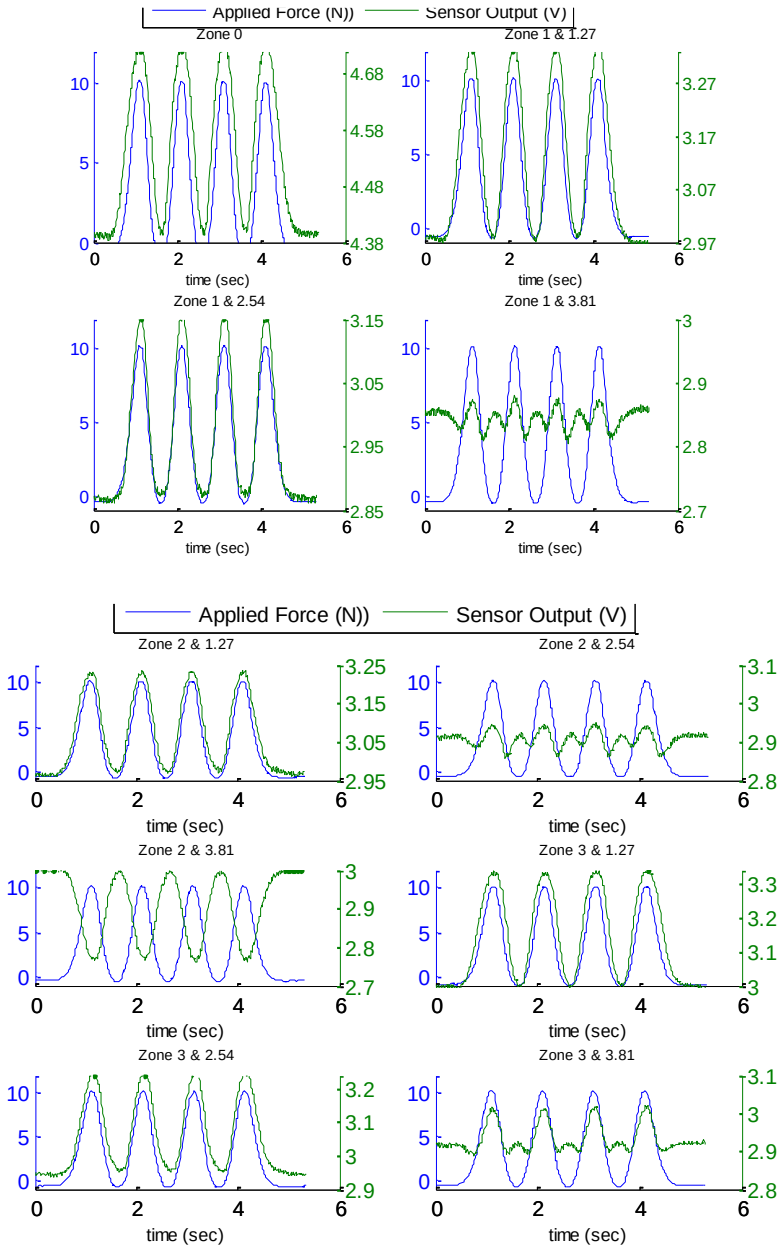

Figure 49 - NMP (1 Layer) Sensor: Force Application at – a) Zone 0 and Zone 1, b) Zone 2 and Zone 3

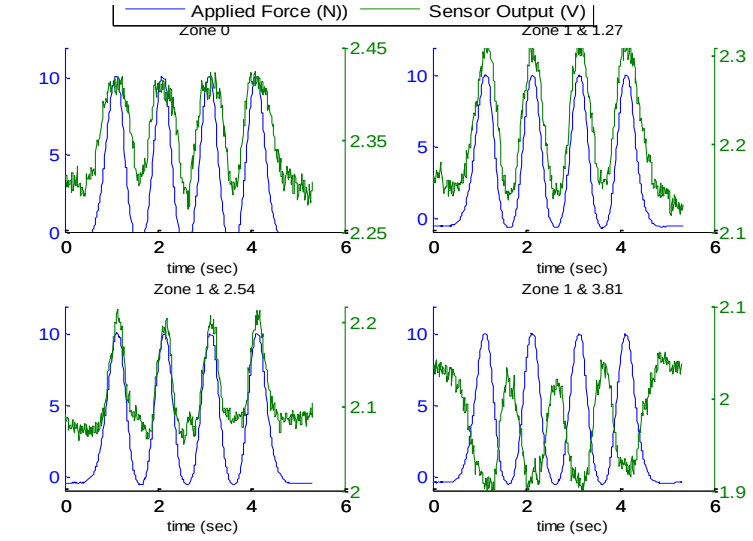

a)

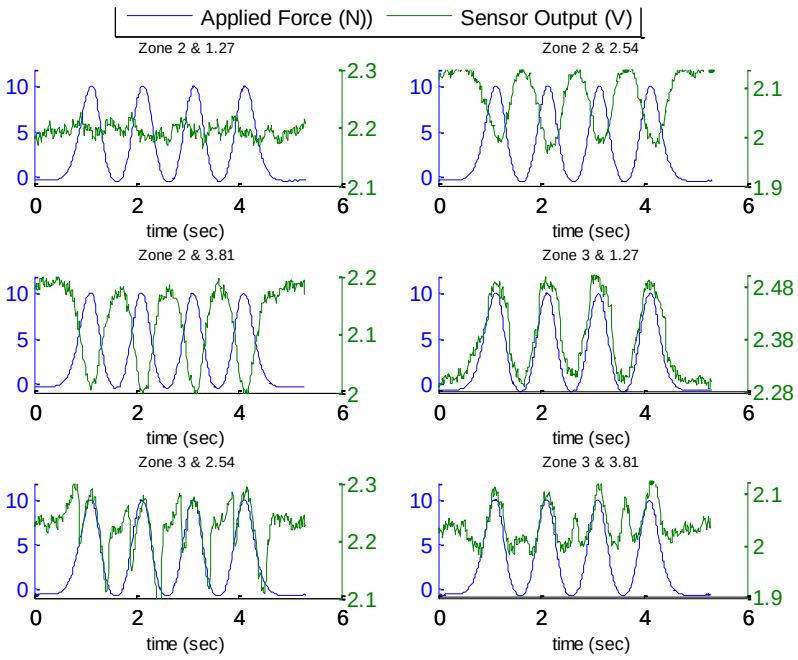

b)

Figure 50 - DMSO (3 Layers) Sensor: Force Application at – a) Zone 0 and Zone 1, b) Zone 2 and Zone 3

NMP (1 Layer) sensor and DMSO (3 Layers) sensor give fairly good response even at zone 0 i.e. when force is applied on top of sensor. Like DMSO (5 Layers) sensor, in zone

1, NMP (5 Layers) sensor's response degrades slightly as we go on changing in the position and move away from sensor module. This is similar in case of DMSO (3 Layers) as well which is shown Figure 50. But, NMP (1 Layer) sensor behaves differently in zone 1 region as its responds consistently well in zone 1 positions except at 3.81mm position.

Similar to DMSO (5 Layer) sensor, NMP (5 Layer) sensor gives fairly good responses in zone 2 which are inversely proportional to applied force trajectory. Also, in zone 2, as we go away from the sensor, it keeps improving the output response. In case of zone 3, considering NMP (5 Layer) and DMSO (3 Layer) sensors, output response degrades as we keep going away from sensor and apply force at each position. In contradiction to this, using NMP (1 Layer) and DMSO (5 Layers), output response from sensor was better in zone 3 compared to other sensors, even if we change the position and apply the force away from sensor.

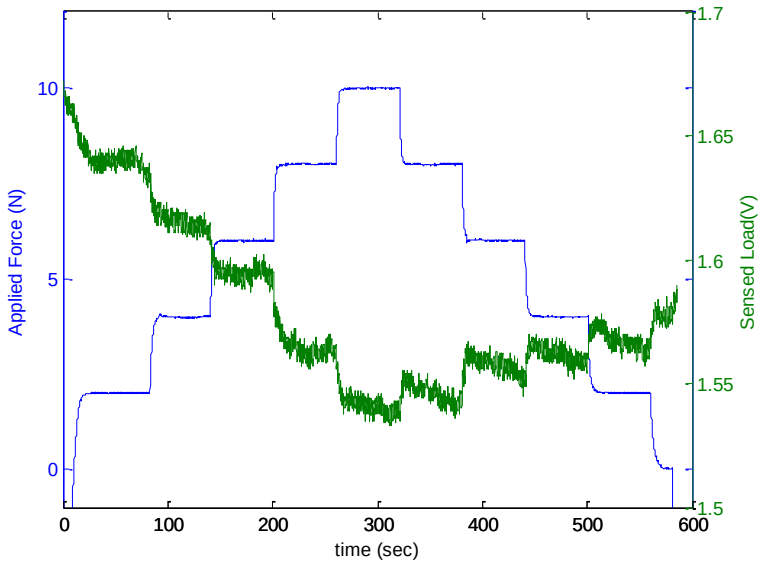

Figure 51 – Static Experiment on Pressure Sensor with bottom and top skins

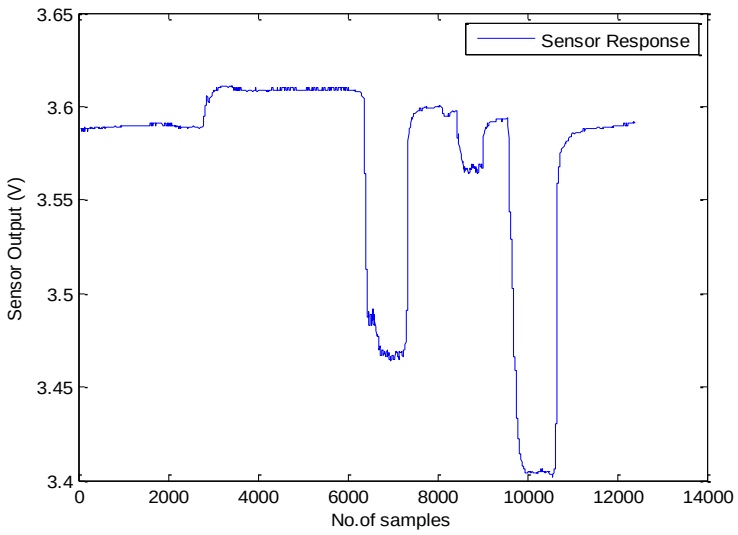

Figure 52 – Static Experiment on Pressure Sensor without skins

Static experiments were performed by applying incrementally increasing force (10 Newton maximum) on top pressure sensor as well as in three different zones (zone 1, zone 2 and zone 3). For all the experiments, stepwise force increment of 2 Newton was applied and at each step force was kept constant for the duration of 1 minute. As an example, static experiments performed on PEDOT: NMP (1 Layer) sensor, with 4mm P10 polymer at bottom and 2mm P10 polymer skin at top of a pressure sensor, is shown in Figure 51. Green curve shows the sensed output from sensor module and blue curve represents the applied force trajectory. Figure 52 shows response from a pressure, without any skins at top and at bottom of sensor, for a random application of static forces.

The output response from sensor with skins at top and underneath a sensor module differed considerably when compared that with no skins. When no skins were used, sensor output was able to reach its steady state value after releasing the pressure applied on sensor module (Figure 52). However, when skin patches were placed at bottom and top of sensor, the response obtained from senor was different than that with

no skin patches used. Even after releasing the pressure, sensor output was unable to reach its steady state and kept decreasing by small amount (Figure 51). This reflects, that the skin patches make impact on output if placed at bottom and top of pressure sensor. Although sensor output was not reaching to its steady state or reference value, it would be interesting to see how it was following the applied force trajectory. For each increasing step of applied force, sensor output dropped down by certain amount showing linear relation to applied input trajectory.

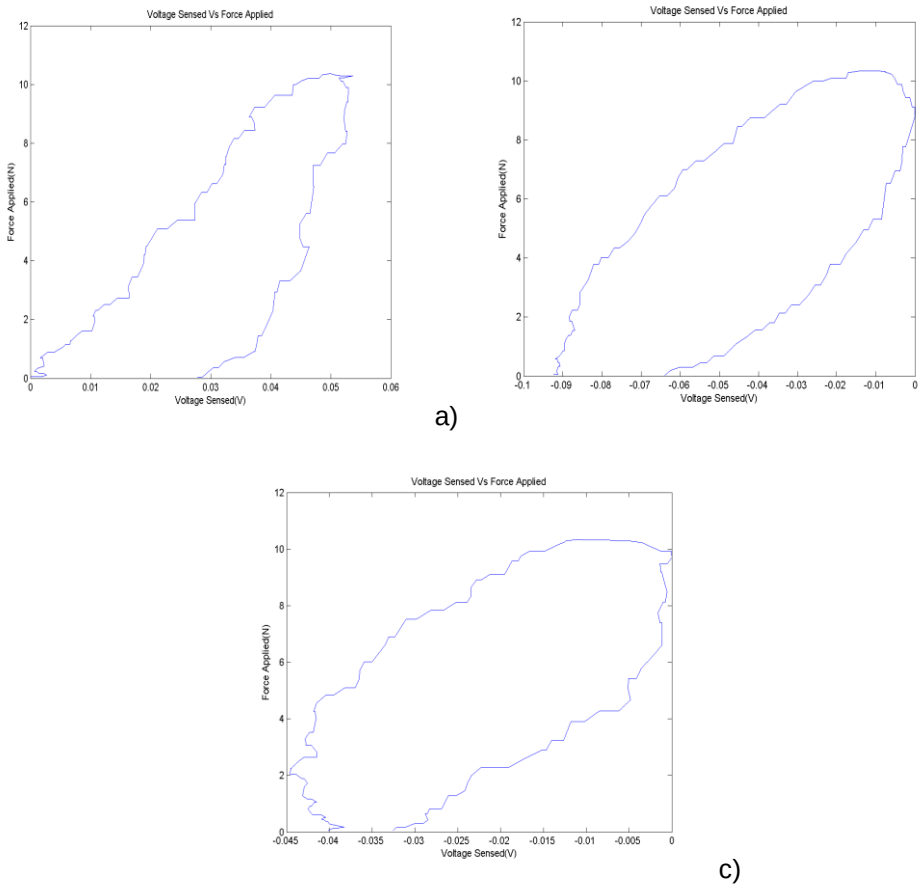

Figure 53 – PEDOT: DMSO (5Layers) Cyclic curve response at different positions - a) At 0mm, b) At zone1: 1.27mm, c) zone 1: 3.81mm

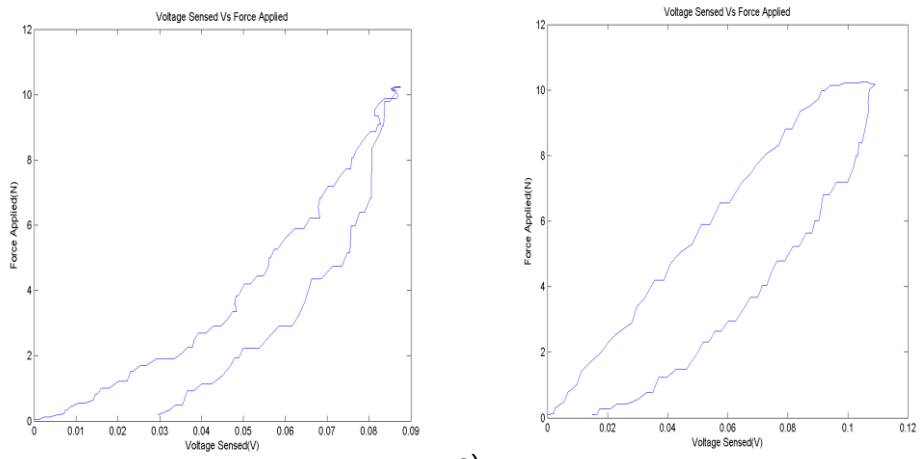

Figure 54 – PEDOT: NMP (5Layers) Cyclic curve response at different positions - a) At 0mm, b) At zone1: 1.27mm, c) zone 1: 3.81mm

Figure 53 shows the cyclic curve responses obtained for PEDOT: DMSO (5 Layers) sensor module whereas Figure 54 shows cyclic curve responses obtained for PEDOT: NMP (5 Layers) sensor module. For both sensors, force was applied at different positions such as – on top of sensor zone 0 (0 mm), zone 1: 1.27mm and at zone1: 3.81mm. Cyclic curve responses were obtained for relationship between applied force and sensed voltage. It can be seen that, for both the sensors, the relationship is quite

linear. Also, the responses from both the sensors are consistent for the positions where the force was applied.

		DMSO 5 Layers 4mm P10 Bottom					
		4mmP10		4mmFrubber		2mmP10	
		Area under Cyclic curve	Correlation coefficient	Area under Cyclic curve	Correlation coefficient	Area under Cyclic curve	Correlation coefficient
Zone 0	0mm	0.215	0.729	0.046	0.839	0.015	0.791
	1.27mm	0.499	0.728	0.425	0.809	0.250	0.858
Zone 1	2.54mm	0.360	0.838	0.272	0.602	0.265	0.862
	3.81mm	0.256	0.680	0.239	0.835	0.121	0.791
	1.27mm	0.111	0.403	0.428	0.763	0.338	0.746
Zone 2	2.54mm	0.209	0.781	0.981	0.781	0.645	0.831
	3.81mm	0.338	0.812	1.235	0.666	0.845	0.838
	1.27mm	0.278	0.732	0.206	0.647	0.027	0.513
Zone 3	2.54mm	0.298	0.849	0.617	0.817	0.480	0.862
	3.81mm	0.301	0.872	0.557	0.848	0.450	0.852
Average		0.287	0.742	0.501	0.761	0.344	0.794

a)

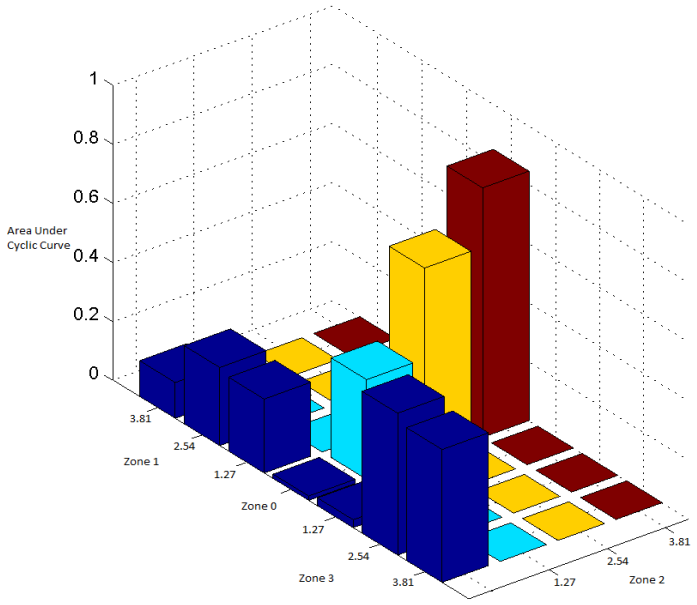

b)

Figure 55 - DMSO (5 Layers) 4mmP10Bottom: a) Statistical Analysis, b) 3D representation for Area under Cyclic Curve with 2mm P10 Top

To verify the comparison results, statistical analysis was carried out to get the area covered under cyclic curve showing the difference between load applied on sensors

and load sensed. The area under cyclic curve was calculated using MATLAB® function ‘trapz’ which uses trapezoidal method to obtain numerical integration. This function divides area under cyclic curve into subintervals and approximates each subinterval by trapezoid. The smaller the area under total cyclic curve, the better the sensor response for applied force.

Also, the correlation coefficient was calculated for each experiment which is the quantitative measure of correlation between applied load and sensed load from pressure sensors. MATLAB® correlation function ‘corr(x,y)’ was used to calculate correlation coefficient between applied force and sensor output data. Correlation coefficient tells us how strong a relationship is between two data sets. Correlation function returns a value of correlation coefficient between 1 and -1 where, 1 indicates strong positive relationship, -1 indicates strong negative relationship and value 0 indicates poor relationship between applied force and sensor output in our case. For simplicity, we have considered an absolute value of correlation coefficients. Greater the absolute value of a correlation coefficient, the stronger the linear relationship between applied force and sensor response.

Based on two criteria, combinations of different skin bottoms, skin tops and sensor types for each skin combination were compared and statistically analyzed to choose the best possible combination of skin and sensor types. Figure 55 and Figure 56 show how the quantitative analysis done for PEDOT: DMSO (5 Layers) with 4mmP10 bottom and 4mm Frubber® bottom, respectively. The analysis was done for 4mm P10 and 4mm Frubber® at bottom and combination of three skins at top.

		DMSO 5 Layers 4mm Frubber Bottom					
		4mmP10		4mmFrubber		2mmP10	
		Area under Cyclic curve	Correlation coefficient	Area under Cyclic curve	Correlation coefficient	Area under Cyclic curve	Correlation coefficient
Zone 0	0mm	1.483	0.537	2.178	0.693	1.270	0.644
	1.27mm	1.381	0.620	2.085	0.687	1.140	0.632
Zone 1	2.54mm	1.148	0.737	1.479	0.702	1.017	0.722
	3.81mm	0.926	0.762	0.453	0.309	0.802	0.674
	1.27mm	0.958	0.281	0.790	0.619	0.526	0.407
Zone 2	2.54mm	0.172	0.593	0.045	0.594	0.212	0.693
	3.81mm	0.567	0.740	0.985	0.641	0.684	0.720
	1.27mm	1.526	0.275	2.199	0.655	1.528	0.634
Zone 3	2.54mm	1.527	0.537	2.074	0.642	1.554	0.623
	3.81mm	1.308	0.596	1.586	0.654	1.402	0.706
Average		1.100	0.568	1.387	0.619	1.014	0.645

a)

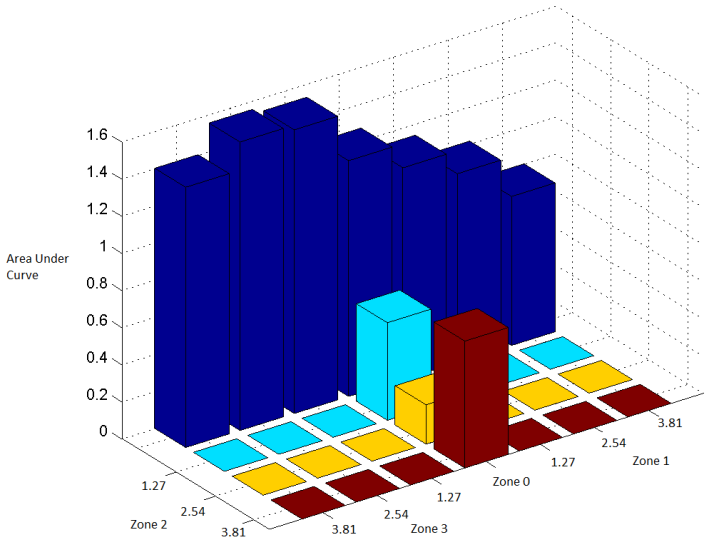

b)

Figure 56 – DMSO (5 Layers) 4mmFrubberBottom: a) Statistical Analysis, b) 3D representation for Area under Cyclic Curve with 2mm P10 Top

		NMP 5 Layers		4mm P10 Bottom	
		4mmP10		2mmP10	
		Area under Cyclic curve	Correlation coefficient	Area under Cyclic curve	Correlation coefficient
Zone 0	0mm	0.132	0.926	0.181	0.915
	1.27mm	0.309	0.909	0.528	0.910
Zone 1	2.54mm	0.331	0.906	0.601	0.875
	3.81mm	0.119	0.910	0.052	0.124
	1.27mm	0.040	0.976	0.349	0.545
Zone 2	2.54mm	0.367	0.349	0.844	0.702
	3.81mm	0.482	0.620	0.931	0.707
	1.27mm	0.164	0.905	0.229	0.927
Zone 3	2.54mm	0.190	0.920	0.550	0.909
	3.81mm	0.053	0.954	0.371	0.827
Average		0.219	0.837	0.464	0.744

a)

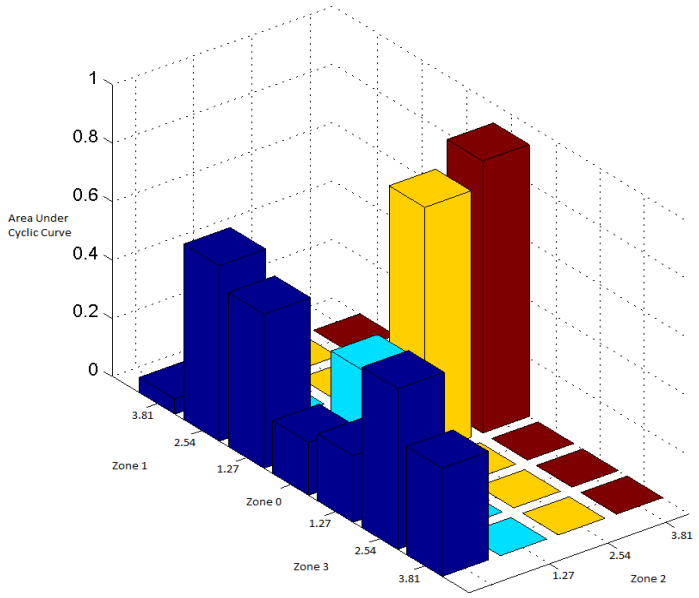

b)

Figure 57 - – NMP (5 Layers) 4mmP10Bottom: a) Statistical Analysis, b) 3D representation for Area under Cyclic Curve with 2mm P10 Top

For each zone i.e. zone 0 to zone 3 with each skin combination, the area under cyclic curve and the correlation coefficient was calculated and tabulated. The higher the value of correlation coefficient, and the lower the value of area under cyclic curve, better

is the response. The highlighted part shows the lowest and highest values for area under the curve and correlation coefficient, respectively, and average values were calculated, for each column.

		NMP 5 Layers		4mm Frubber Bottom	
		4mmP10		2mmP10	
		Area under Cyclic curve	Correlation coefficient	Area under Cyclic curve	Correlation coefficient
Zone 0	0mm	0.486	0.541	1.801	0.682
	1.27mm	1.326	0.608	1.777	0.587
Zone 1	2.54mm	1.711	0.624	1.565	0.809
	3.81mm	1.822	0.562	1.561	0.753
	1.27mm	0.457	0.570	0.854	0.679
Zone 2	2.54mm	0.084	0.487	0.228	0.377
	3.81mm	0.085	0.536	0.843	0.703
	1.27mm	0.419	0.202	1.850	0.712
Zone 3	2.54mm	0.059	0.456	1.277	0.764
	3.81mm	1.155	0.505	1.046	0.805
Average		0.760	0.509	1.280	0.687

a)

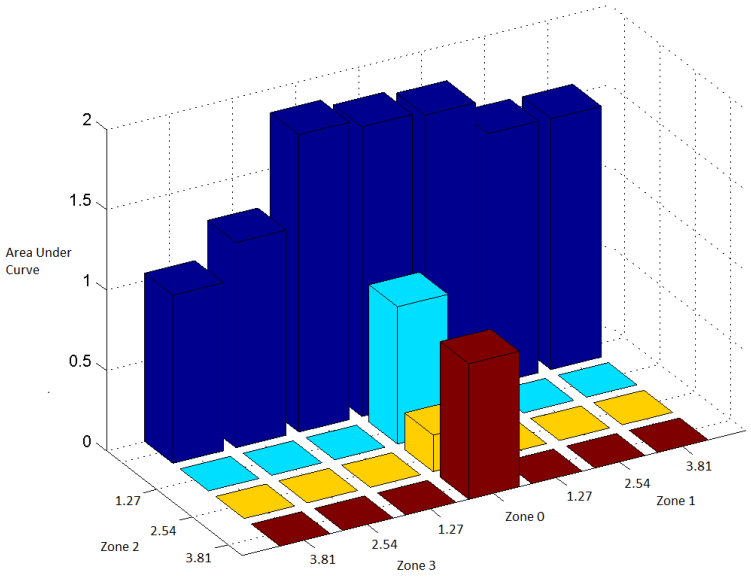

b)

Figure 58 - – NMP (5 Layers) 4mmFrubberBottom: a) Statistical Analysis, b) 3D representation for Area under Cyclic Curve with 2mm P10 Top

The analysis done for PEDOT: NMP (5 Layers) sensor is shown in Figure 57 and Figure 58. If carefully observe the results obtained for PEDOT: DMSO (5 Layers) and PEDOT: NMP (5 Layers), it would be interesting to see that, both sensors operate differently in different zones. Each highlighted part indicates best possible performance for that particular column or combination of skin materials. Considering the averages obtained for each criteria and for each skin combination, 4mm P10 polymer, when placed at the bottom of pressure sensor, performs better compared to 4mm Frubber® bottom in terms of area under cyclic curve and correlation coefficient. This is true for both DMSO and NMP sensors. For example, average area under cyclic curve and average correlation coefficient for DMSO (5 layers) with 4mm P10 bottom are 0.287 and 0.742 respectively whereas that with 4mm Frubber® bottom are 1.099 and 0.567. This clearly shows that average area under the curve is lesser and correlation coefficient is more using 4mm P10 polymer at bottom compared to 4mm Frubber® bottom reflecting 4mm P10 polymer bottom as a better option. In a similar way it can be identified, that with 4mm P10 as a skin top, we can consistently get better results when compared to that with 2mm P10 polymer and 4mm Frubber® skins at top of sensor module. Similar quantitative analysis for DMSO (3 Layers) sensor is shown Figure 59 and Figure 60 , and that for NMP (1 Layer) sensor is shown in Figure 61 and Figure 62.

		DMSO 3 Layers 4mm P10 Bottom					
		4mmP10		4mmFrubber		2mmP10	
		Area under Cyclic curve	Correlation coefficient	Area under Cyclic curve	Correlation coefficient	Area under Cyclic curve	Correlation coefficient
Zone 0	0mm	0.381	0.827	0.507	0.781	0.314	0.804
	1.27mm	0.389	0.842	0.766	0.786	0.615	0.826
Zone 1	2.54mm	0.383	0.833	0.276	0.634	0.521	0.860
	3.81mm	0.080	0.873	1.000	0.689	0.425	0.769
	1.27mm	0.168	0.898	0.208	0.360	0.099	0.054
Zone 2	2.54mm	0.133	0.532	0.850	0.677	0.672	0.755
	3.81mm	0.337	0.557	0.758	0.704	0.824	0.758
	1.27mm	0.411	0.839	0.767	0.827	0.695	0.723
Zone 3	2.54mm	0.509	0.864	0.767	0.782	0.367	0.446
	3.81mm	0.421	0.834	1.258	0.259	0.493	0.709
Average		0.321	0.790	0.716	0.650	0.502	0.671

a)

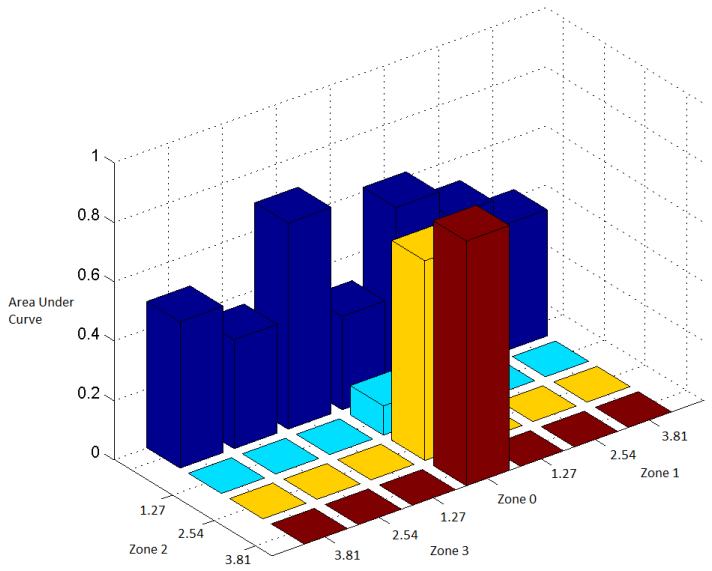

b)

Figure 59 - DMSO (3 Layers) 4mmP10Bottom: a) Statistical Analysis, b) 3D representation for Area under Cyclic Curve with 2mm P10 Top

				DMSO 3 Layers	4mm Frubber Bottom		
		4mmP10		4mmFrubber		2mmP10	
		Area under Cyclic curve	Correlation coefficient	Area under Hysteresis	Area under Cyclic curve	Area under Cyclic curve	Correlation coefficient
Zone 0	0mm	1.289	0.763	2.045	0.680	1.175	0.684
	1.27mm	1.273	0.751	1.936	0.747	1.014	0.780
Zone 1	2.54mm	1.119	0.812	1.578	0.796	1.145	0.783
	3.81mm	0.724	0.882	1.064	0.693	1.001	0.786
	1.27mm	0.820	0.573	0.946	0.671	0.578	0.720
Zone 2	2.54mm	0.023	0.551	0.124	0.411	0.026	0.098
	3.81mm	0.685	0.684	1.105	0.640	0.736	0.687
	1.27mm	1.252	0.700	1.830	0.678	1.326	0.721
Zone 3	2.54mm	1.156	0.681	1.497	0.709	1.273	0.730
	3.81mm	0.911	0.802	1.542	0.687	1.085	0.757
Average		0.925	0.720	1.367	0.671	0.936	0.675

a)

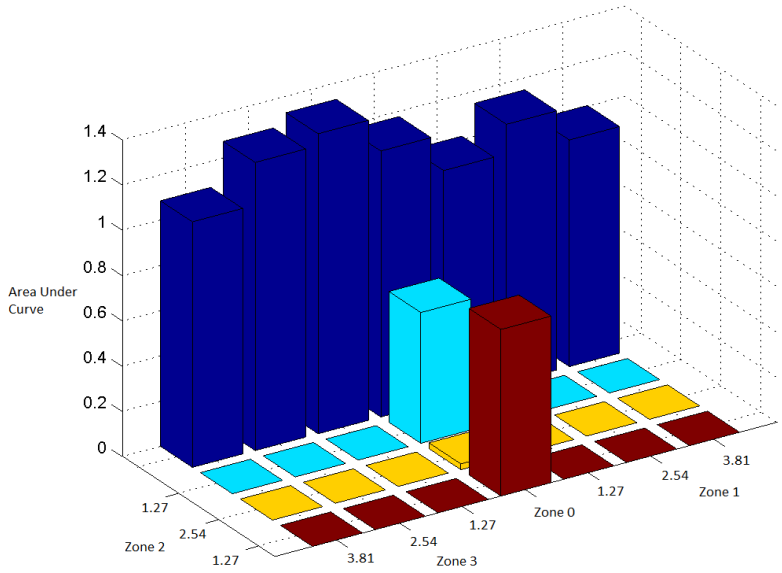

b)

Figure 60 - DMSO (3 Layers) 4mmFrubberBottom: a) Statistical Analysis, b) 3D representation for Area under Cyclic Curve with 2mm P10 Top

		NMP 1 Layer	4mm P10 Bottom		
4mmP10		4mmFrubber		2mmP10	
Area under Cyclic curve	Correlation coefficient	Area under Cyclic curve	Correlation coefficient	Area under Cyclic curve	Correlation coefficient
0.994	0.723	2.036	0.731	0.875	0.861
0.739	0.866	1.779	0.817	1.062	0.875
0.577	0.886	0.700	0.859	1.295	0.770
0.187	0.902	0.418	0.414	0.029	0.620
0.536	0.878	1.100	0.819	0.762	0.894
0.129	0.963	0.613	0.446	0.040	0.781
0.321	0.471	1.445	0.717	1.063	0.760
0.790	0.831	1.568	0.806	1.048	0.840
0.621	0.818	1.237	0.809	1.100	0.852
0.362	0.768	0.317	0.555	0.468	0.770
0.526	0.810	1.121	0.697	0.774	0.802

a)

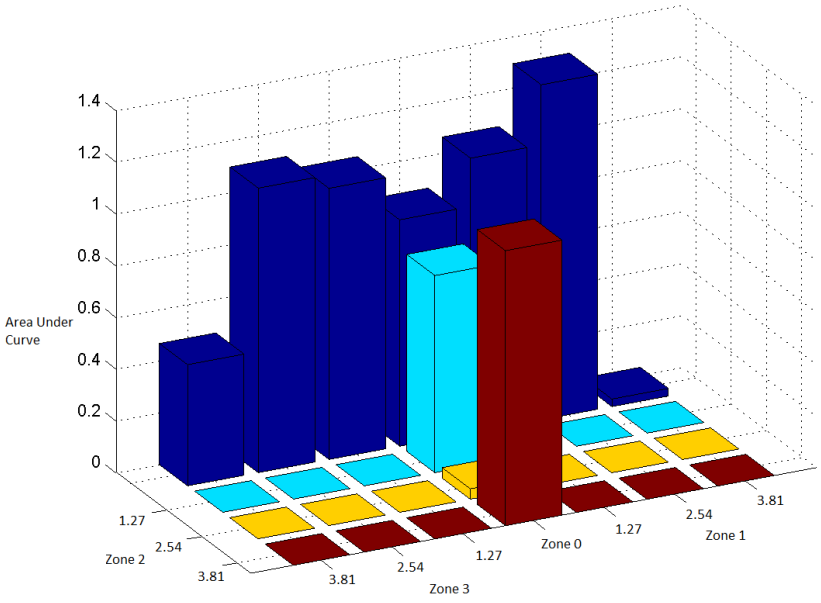

b)

Figure 61 - NMP (1 Layer) 4mmP10Bottom: a) Statistical Analysis, b) 3D representation for Area under Cyclic Curve with 2mm P10 Top

				NMP 1 Layer	4mm Frubber Bottom		
		4mmP10		4mmFrubber		2mmP10	
		Area under Cyclic curve	Correlation coefficient	Area under Cyclic curve	Correlation coefficient	Area under Cyclic curve	Correlation coefficient
Zone 0	0mm	3.202	0.570	3.424	0.696	1.524	0.723
	1.27mm	2.872	0.721	3.249	0.729	1.838	0.740
Zone 1	2.54mm	2.778	0.764	3.351	0.762	1.964	0.774
	3.81mm	2.230	0.789	2.570	0.748	1.607	0.776
	1.27mm	2.317	0.718	2.857	0.711	1.896	0.766
Zone 2	2.54mm	1.708	0.764	2.074	0.754	1.422	0.831
	3.81mm	0.638	0.457	0.049	0.196	0.698	0.576
	1.27mm	2.861	0.720	3.345	0.690	2.121	0.693
Zone 3	2.54mm	2.342	0.738	3.260	0.626	1.599	0.731
	3.81mm	1.564	0.748	2.498	0.675	1.101	0.758
Average		2.251	0.699	2.668	0.659	1.577	0.737

a)

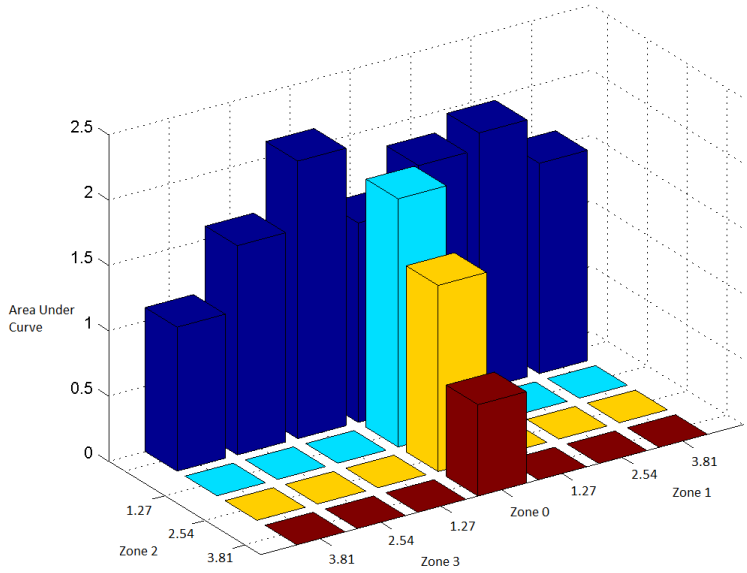

b)

Figure 62 - NMP (1 Layer) 4mmFrubberBottom: a) Statistical Analysis, b) 3D representation for Area under Cyclic Curve with 2mm P10 Top

Chapter 5

Conclusion and Future Work

5.1 Conclusion

In this thesis, we presented the work related to piezoresistive pressure sensor manufacturing, testing and its characterization. The importance of tactile sensing modules for robots and the motivation behind the integration of an electronic skins on the robots were presented in this thesis. During this work, we studied and a reduced order model relating the applied and sensed forces and conducted the experiments to identify the parameters which will be used in SkinSim simulation environment. Also, we discussed and studied novel techniques to obtain risk free physical human-robot interaction (pHRI) which is of high importance and becoming inevitable in our day to day life.

The existing experimental setup was dedicated to test some commercial sensor modules. We studied and modified the experimental setup in order to characterize the newly developed piezoresistive pressure sensors. The hardware which includes NI cRIO controller, Servo motor, linear actuator, servo drive interface, analog input module, was dedicated to perform different tests on sensor modules. According to the requirements of pressure sensors, the hardware was modified to get the real time response from sensors. The plunger attached to the linear actuator was used to apply force on piezoresistive pressure sensors. The problem with previous analog input module was that its 12 bit resolution. As per the need of our sensors, the existing low resolution analog input module had to be replaced by a 16-bit resolution module.

Another problem was, no dedicated hardware was available to read the data from high resolution piezoresistive pressure sensors. When force was applied on sensors, their resistance changed by small amount, which was very difficult to measure

with existing circuitry. To read the smallest change in resistance, a circuit was developed which consisted of Wheatstone bridge, an operation amplifier and other supporting hardware.

We studied the control algorithm in order to obtain risk free interaction between robots and environment. Various control techniques, including explicit force control and impedance control, were discussed and implemented using LabVIEW and MATLAB. The limitations and advantages of force control schemes were discussed and successfully implemented them on actual hardware.

As a part of manufacturing process, Electrohydrodynamic (EHD) ink jet printing method was studied and implemented on pressure sensors. The printing process has to be implemented to make the sensors conductive. PEDOT: PSS piezoresistive material was used as a conductive material. Two types of inks were prepared by mixing two different ink solvents to PEDOT: PSS, they are – 1) NMP and 2) DMSO. The sensors were printed using two inks were made ready for testing and characterization.

The sensors were packaged with two different skins – P10 silicone polymer and Frubber ® skin. The structure and features of both skin were studied which helped to test the sensors in a better way. Different combinations of skin samples were used on top and bottom of pressure sensors. To better understand sensor's behavior, different static and dynamic tests were performed by applying incrementally increasing force on top of the sensor and skin patch.

It was observed that the pressure sensor response tends to drift a lot even at resting position. The primary factors involved with sensor drifting were the drift in driver hardware used and the environmental conditions such as temperature.

Sensor placement was another factor to carefully control while conducting experiments. We had to place and fix the sensors at a measured position marked by X-Y

stage scale. For this reason, a dedicated 3D printed test fixture was developed. The idea behind test fixture was, that the sensor will be positioned and aligned in a proper way so that it should not move and misalign during experimental tests.

After setting up the all the required hardware, we performed extensive testing on piezoresistive pressure sensors. Different sensors, classified based on ink material, number of layers used to EHD print, bottom and top skin materials and thicknesses were tested and compared. After data analysis, we drew some conclusions as follows:

- Frubber® skin material experiences more drift and hysteresis than that with P10 polymer skin, when placed at the bottom and/or top of pressure sensor. As Frubber® skin is very soft, sensor output shows largely nonlinear behavior. Senor output takes time to reach to its reference voltage value after releasing the applied pressure on sensor covered with Frubber® skin.
- On the other hand P10 silicone polymer skin is more elastic and harder than Frubber® skin material and exhibits liner behavior. For PEDOT: NMP (5 Layers) sensor, the combination of 4mm P10 polymer bottom and 4mm P10 polymer skin top works best. For PEDOT: DMSO (5 Layers) sensor, the combination of 4mm P10 polymer bottom and 2mm P10 polymer skin top works best. Sensor response also depends on the position at which force was applied.
- As discussed earlier, experiments were performed in four different zones – zone 0 to 3. Unlike zone 1 and zone 3, in zone 2, senor output varies in inverse proportion with applied force. Although it behaves differently, results obtained with zone 2 were consistent in terms of both linearity and amount of voltage sensed for all sensors.
- Sensors were also compared based on number of ink layers used to EHD print on them. Using PEDOT: NMP (1 Layer) with 4mm P10 polymer skin at bottom, better

average change in sensed voltage was obtained when compared that with PEDOT: NMP (5 layers), in all the zones.

- After performing static tests with skins patches at top and bottom of pressure sensor, it was identified, that sensor output voltage continuously drops as soon as force is applied on sensor. Also, the output does not to reach its steady state or reference value even when pressure on sensor was released or reduced. On the other hand, if no polymer skins were used, sensor output goes back to its reference value when pressure is released. This suggests that the bulk of the hysteretic behavior of the sensor is due to polymer encapsulation, and not the sensor ink material.

5.2 Future Work

Future research work should include more testing and characterization of pressure sensors of same type in order to prove their repeatability. It is important to redesign the experimental setup in a better manner so as to reduce any drifting effects in ouptut response of sensor due to hardware. For this thesis, manual X-Y stage was used as a base and to place the electronic skins,but in future it will be beneficial to replace the manual X-Y stage with automated stage. It will not only improve the speed and accuracy but also the repeatability.

Software was developed to automate the testing and characterization process. In future it will be helpful to make some improvements in software and increase the speed of operation. Also, different control algorithms were developed but only explicit force control technique was applied on actual sensors. Although an explicit force control works well for experiments performed in this thesis, it would be interesting to see how an impedance control scheme works when used in sensor testing process.

References

[1] R. S. Dahiya, G. Metta, M. Valle and G. Sandini, "Tactile sensing—from humans to humanoids," *Robotics, IEEE Transactions on,* vol. 26, no. 1, pp. 1-20, 2010.

[2] C. Wang, D. Hwang, Z. Yu, K. Takei, J. Park, T. Chen, B. Ma and A. Javey, "User-interactive electronic skin for instantaneous pressure visualization," *Nature materials,* vol. 12, no. 10, pp. 899-904, 2013.

[3] "Research | Javey Group - Electronic Skin," [Online]. Available: http://nano.eecs.berkeley.edu/research/eskin.html.

[4] Y. Li, M. Yuan and J. Xu, "A pressure sensor study and research," in *Computing, Control and Industrial Engineering (CCIE), 2011 IEEE 2nd International Conference on*, 2011.

[5] J. Park, Y. Lee, J. Hong, Y. Lee, M. Ha, Y. Jung, H. Lim, S. Y. Kim and H. Ko, "Tactile-Direction-Sensitive and Stretchable Electronic Skins Based on Human-Skin-Inspired Interlocked Microstructures," *ACS nano,* vol. 8, no. 12, pp. 12020-12029, 2014.

[6] A. Habib, I. Ranatunga, K. Shook and D. O. Popa, "SkinSim: A simulation environment for multimodal robot skin," in *Automation Science and Engineering (CASE), 2014 IEEE International Conference on*, 2014.

[7] K. R. Shook, A. Habib, W. H. Lee and D. O. Popa, "Experimental testbed for robot skin characterization and interaction control," in *SPIE Sensing Technology+ Applications*, 2014.

[8] S. Stassi, V. Cauda, G. Canavese and C. F. Pirri, "Flexible tactile sensing based on piezoresistive composites: a review," *Sensors,* vol. 14, no. 3, pp. 5296-5332, 2014.

[9] H. Yu and J. Huang, "Design and Application of a High Sensitivity Piezoresistive Pressure Sensor for Low Pressure Conditions," *Sensors,* vol. 15, no. 9, pp. 22692-22704, 2015.

[10] "Sensor Fundamentals," [Online]. Available: http://www.mfg.mtu.edu/cyberman/machtool/machtool/sensors/fundamental.html.

[11] J. Shin, W. H. Lee, C. P. Nothnagle and M. B. Wijesundara, "EHD as sensor fabrication technology for robotic skins," in *SPIE Sensing Technology+ Applications*, 2014.

[12] "Highly sensitive flexible pressure sensors with microstructured rubber dielectric layers," [Online]. Available: http://www.nature.com/nmat/journal/v9/n10/full/nmat2834.html.

[13] "High-Tech Robot Skin," [Online]. Available: http://www.nasa.gov/vision/earth/everydaylife/vladskin.html.

[14] B. C. Tee, C. Wang, R. Allen and Z. Bao, "An electrically and mechanically self-healing composite with pressure-and flexion-sensitive properties for electronic skin applications," *Nature nanotechnology,* vol. 7, no. 12, pp. 825-832, 2012.

[15] L. Seminara, L. Pinna, A. Ibrahim, L. Noli, M. Capurro, S. Caviglia, P. Gastaldo and M. Valle, "Electronic Skin: achievements, issues and trends," *Procedia Technology,* vol. 15, pp. 550-559, 2014.

[16] S. Wagner, S. P. Lacour, J. Jones, I. H. Pai-hui, J. C. Sturm, T. Li and Z. Suo, "Electronic skin: architecture and components," *Physica E: Low-dimensional Systems and Nanostructures,* vol. 25, no. 2, pp. 326-334, 2004.

[17] "Make Awesome: The Story of Elastic Electronic Skin - The Berkeley Science Review," [Online]. Available: http://berkeleysciencereview.com/make-awesome-the-story-of-elastic-electronic-skin/.

[18] P. Mittendorfer and G. Cheng, "Humanoid multimodal tactile-sensing modules," *Robotics, IEEE Transactions on,* vol. 27, no. 3, pp. 401-410, 2011.

[19] P. Mittendorfer and G. Cheng, "Integrating discrete force cells into multi-modal artificial skin," in *Humanoid Robots (Humanoids), 2012 12th IEEE-RAS International Conference on*, 2012.

[20] P. Mittendorfer, "From a Multi-modal Intelligent Cell to a Self-organizing Robotic Skin-Realizing Self and Enriching Robot Tactile Interaction," 2015.

[21] S. Katsura, Y. Matsumoto and K. Ohnishi, "Analysis and experimental validation of force bandwidth for force control," *Industrial Electronics, IEEE Transactions on,* vol. 53, no. 3, pp. 922-928, 2006.

[22] S. Chiaverini and L. Sciavicco, "The parallel approach to force/position control of robotic manipulators," *Robotics and Automation, IEEE Transactions on,* vol. 9, no. 4, pp. 361-373, 1993.

[23] B. Komati, C. Cl{\'e}vy and P. Lutz, "Force tracking impedance control with unknown environment at the microscale," in *Robotics and Automation (ICRA), 2014 IEEE International Conference on*, 2014.

[24] R. Volpe and P. Khosla, "A theoretical and experimental investigation of explicit force control strategies for manipulators," *Automatic Control, IEEE Transactions on,* vol. 38, no. 11, pp. 1634-1650, 1993.

[25] N. Hogan, "Impedance control: An approach to manipulation: Part II—Implementation," *Journal of dynamic systems, measurement, and control,* vol. 107, no. 1, pp. 8-16, 1985.

[26] N. Hogan, "Stable execution of contact tasks using impedance control," in *Robotics and Automation. Proceedings. 1987 IEEE International Conference on*, 1987.

[27] J. K. Mills, A. Goldenberg and others, "Force and position control of manipulators during constrained motion tasks," *Robotics and Automation, IEEE Transactions on,* vol. 5, no. 1, pp. 30-46, 1989.

[28] F. Almeida, A. Lopes and P. Abreu, "Force-impedance control: a new control strategy of robotic manipulators," *Recent advances in Mechatronics,* pp. 126-137, 1999.

[29] M. H. Raibert and J. J. Craig, "Hybrid position/force control of manipulators," *Journal of Dynamic Systems, Measurement, and Control,* vol. 103, no. 2, pp. 126-133, 1981.

[30] G. J. Garcia, J. A. Corrales, J. Pomares and F. Torres, "Survey of visual and force/tactile control of robots for physical interaction in Spain," *Sensors,* vol. 9, no. 12, pp. 9689-9733, 2009.

[31] Y. Zhu and E. J. Barth, "Impedance control of a pneumatic actuator for contact tasks," in *Robotics and Automation, 2005. ICRA 2005. Proceedings of the 2005 IEEE International Conference on*, 2005.

[32] K.-H. Choi, A. Khan, H.-C. Kim, K. Rahman, K.-R. Kwon, N. M. Muhammad and Y.-H. Doh, Electrohydrodynamic inkjet-micro pattern fabrication for printed electronics applications, INTECH Open Access Publisher, 2011.

[33] "Ceramics - Research." Princeton University," [Online]. Available: http://www.princeton.edu/~cml/html/research/ehdp.html.

[34] "ijetae," [Online]. Available: http://www.ijetae.com/files/Volume4Issue5/.

[35] A. N. Das, P. Zhang, W. H. Lee, D. Popa and H. Stephanou, "μ 3: multiscale, deterministic micro-nano assembly system for construction of on-wafer microrobots," in *Robotics and Automation, 2007 IEEE International Conference on*, 2007.

[36] "NI cRIO-9074," [Online]. Available: http://sine.ni.com/nips/cds/view/p/lang/en/nid/203964.

[37] "NI 9516 C Series Servo Drive Interface with Dual Encoder Feedback," [Online]. Available: http://sine.ni.com/nips/cds/view/p/lang/en/nid/206349.

[38] "NI 9205 32-Ch ±200 mV to ±10 V, 16-Bit, 250 kS/s Analog Input Module," [Online]. Available: http://sine.ni.com/nips/cds/view/p/lang/en/nid/208800.

[39] L. K. Wells and J. Travis, LabVIEW for everyone: graphical programming made even easier, Prentice-Hall, Inc., 1996.

[40] C. Elliott, V. Vijayakumar, W. Zink and R. Hansen, "National instruments LabVIEW: a programming environment for laboratory automation and measurement," *Journal of the Association for Laboratory Automation,* vol. 12, no. 1, pp. 17-24, 2007.

[41] "Maxon servo amplifier," [Online]. Available: http://www.farnell.com/datasheets/1642526.pdf.

[42] A. Devices, "Single-Supply, Rail-to-Rail, Low Cost, Instrumentation Amplifier," *AD623 datasheet,* 2008.

[43] G. Latessa, F. Brunetti, A. Reale, G. Saggio and A. Di Carlo, "Piezoresistive behaviour of flexible PEDOT: PSS based sensors," *Sensors and Actuators B: Chemical,* vol. 139, no. 2, pp. 304-309, 2009.

[44] B. Komati, M. R. Pac, I. Ranatunga, C. Cl{\'e}vy, D. O. Popa and P. Lutz, "Explicit force control vs impedance control for micromanipulation," in *ASME 2013 International Design Engineering Technical Conferences and Computers and Information in Engineering Conference*, 2013.

[45] [Online]. Available: http://www.medgadget.com/2010/09/stanfords_rubber_based_artificial_skin.html.

[46] F. Ikhouane and J. Rodellar, Systems with hysteresis: Analysis, identification and control using the Bouc-Wen model, John Wiley \& Sons, 2007.

[47] "Temperature effects," [Online]. Available: http://www.ni.com/white-paper/3432/en/.

[48] K. Hoffmann, "Applying the Wheatstone Bridge Circuit," *HBM S1569-1.1 en, HBM, Darmstadt, Germany, http://www. hbm. com/fileadmin/mediapool/hbmdoc/technical/s1569. pdf,* 2001.

Biographical Information

Ritvij R. Sahasrabuddhe grew up in Mumbai, India. He earned his Diploma in Industrial Electronics from Maharashtra State Board of Technical Education, India in 2010. He successfully completed his Bachelors of Engineering degree in Electronics from Mumbai University, India in 2013 and Master of Science degree in Electrical Engineering from The University of Texas at Arlington in 2015. Ritvij's research interests are in Robotics, and Embedded Systems.